EVALUATION OF PROBABILISTIC SITE-SPECIFIC SEISMIC HAZARD METHODS AND ASSOCIATED UNCERTAINTIES, WITH APPLICATIONS IN THE PO PLAIN, NORTHERN ITALY

E. Faccioli

e.faccioli@studiogeotecnico.it

Scientific Consultant to Studio Geotecnico Italiano, Milan, Italy

Formerly Full Professor at Politecnico di Milano

R. Paolucci

roberto.paolucci@polimi.it

Professor of Earthquake Engineering, Politecnico di Milano, Italy

M. Vanini

mm.vanini@gmail.com

Engineering Consultant

Abstract

Site-specific ground motion hazard assessed by a PSHA one-step approach that handles a single-site sigma and its uncertainties and uses a simple logic tree, is compared with a two-step approach that includes bedrock motion evaluation and wave propagation through a local soil profile with consideration of the main epistemic uncertainties. The one-step analysis relies on

accelerometer data from the Po Plain, a sedimentary basin in Northern Italy where an earthquake sequence with two M_w ~6.0 events occurring in 2012 was extensively recorded. UH spectra on soil and exposed bedrock are evaluated at three deep-soil accelerometer sites (MRN, NVL and T0821), using residual measures available from other studies, by which uncertainties in site terms ($\delta S2S$) and single-site sigma ($\sigma_{ss,s}$) are estimated. Despite similarity in geologic conditions, at least one out of three sites displays in the one-step analysis substantial differences in mean level (T0821) or in the (84-16) percentile spread (NVL), depending on differences in site terms and single-site sigma, possibly caused by source-to site propagation effects.

The two-step approach was applied to the single MRN site using as excitation carefully selected and broadband-matched acceleration signals and linear, equivalent-linear and nonlinear approaches in propagation analyses, finding that assumptions on soil degradation curves dominate the variability of results. The linear approach provided the best results, based on: (i) the similarity of the one-step non-ergodic UHS with the two-step result based on the linear approach; (ii) the comparison with observed records at MRN during the 2012 sequence mainshocks, showing PGA and short period spectral levels well beyond those predicted by different non-linear assumptions; (iii) a similar evidence from a set of 21 stations at deep soil sites of the Japanese Kik-net.

Introduction

Uncertainty components in the PSHA

Recent studies on the aleatory variability and epistemic uncertainty in ground motion prediction have pointed to the conceptual benefits of separating the different types and sources of the uncertainties (Al Atik et al. 2010). Residual analysis of the spectral acceleration prediction equations (GMPEs), applied to extensive regional datasets, have actually shown that when individual sites with recorded data and the associated (non-ergodic) statistical measures of variability are considered, the range of the key uncertainties at play may be reduced with respect to the ergodic case, i.e., when records from many sites are used as is the case with GMPEs. A reduced variability is, in particular, observed for the so-called within-event single-station residual (Rodríguez-Marek et al. 2011 and 2013).

The within-event residual can be regarded as the sum of a site factor, $\delta S2S$, and of a term left after correcting for site and event, δWS_{es}, denoted site- and event-corrected residual (Al Atik et al. 2010, Rodríguez-Marek et al. 2013). The site factor measures the seismic response "personality" of a site; in the words of Al Atik et al. (cit.) "it represents the systematic deviation of the observed amplification at this site from the median amplification predicted by the model using simple site classification such as the average shear-wave velocity in the uppermost 30 meters at the site, VS30". The term δWS_{es}, on the other hand, describes the record-to-record variability of the response at site *s* for earthquake *e*.

The standard deviation, ϕ_{ss}, of δWS_{es} associated to a given dataset was found to be remarkably stable, in that it displays limited variation with respect to magnitude and distance across widely different regional datasets and tectonic environment (Chen and Faccioli, 2013; Rodríguez-Marek et al., 2013), and also to be generally smaller than the ergodic within-event component of the standard deviation associated to the median log prediction of a GMPE. On the other hand, the between-event variability is less easily constrained, as it is significantly source-and path-dependent; it is typically represented by the between-event variability of a regionally based GMPE.

Thus, three main variability components were found to be at play in the previous studies: two of them, denoted as ϕ_{S2S} and ϕ_{ss}, stem from the within-event residuals, and one, denoted as τ, from the between-event residuals. While a traditional PSHA would combine all such components into a single aleatory variability, i.e. the total standard deviation (σ_{logY}) of the adopted GMPEs, Rodríguez-Marek et al. (2014) have argued in favor of separating aleatory variability and epistemic uncertainty, by assuming that the site factor is known, or can be independently calculated (through a site response analysis), and that an epistemic uncertainty should be attached to it. The same authors termed the resulting approach as partially nonergodic and identified as key requirements for its application in PSHA that: (1) the median value of $\delta S2S$ be properly estimated, and both (2) the epistemic uncertainty ϕ_{S2S} in the site term and (3) the epistemic uncertainty ϕ_{ss} in the single-station sigma be taken into account. If, due to lack of recorded data, the site term is independently calculated through a seismic response analysis and ϕ_{S2S} is explicitly taken into account, the two remaining variability measures ϕ_{ss} and τ can be combined into a "single site sigma" σ_{ss}.

Approaches for site-specific PSHA

Although the foregoing concepts allow for considerable refinement of the traditional PSHA tools, with potential reduction of some key uncertainty components, well documented applications to specific sites are still lacking. As a matter of fact, the best example actually deals with a rock site in a stable continental environment (Rodríguez-Marek et al. 2014); the nature of the site and the lack of strong motion records make this case rather unfit for illustrating the potential of a single-site sigma approach to probabilistic site response evaluation in presence of significant soil deposits.

This study explores the actual quantification of the previous residual measures of ground motion predictions and its application to PSHA for deep soil sites in the Po Plain of Northern Italy, a moderate seismicity region where significant strong motion data recorded in the last few years exist.

The data for some representative sites allowed us to estimate the site effect in different ways, leading to different probabilistic site response evaluations. Following Cramer (2003), Bazzurro and Cornell (2004), Perez et al. (2009), the classes of approaches to account for seismic site effects within a PSHA can be broadly classified as summarized in Table 1. Hybrid approaches are typically based on the results of a PSHA at a rock site, where site effects are superimposed by multiplying the uniform hazard spectrum at rock by a suitable site amplification function (SAF). The latter may be defined either by the spectral amplification factors for generic sites introduced typically by seismic norms or guidelines (*HyG*), or by a site-specific SAF, calculated in most cases by considering the mean amplification function from 1D linear-equivalent wave propagation analyses for the specific soil-profile at hand (*HyS*). In such analyses, time-history calculations are normally carried out by considering a suite of real accelerograms, satisfying the response spectrum compatibility with the target PSHA spectrum on rock. While the norm-based *HyG* approach is the one mostly applied for ordinary construction, approach *HyS* is frequently used for site-specific SH analyses of important facilities, and we consider it as the reference hybrid approach for this study.

Fully probabilistic approaches may be classified either as applicable for a generic site (*FpG*) or for a specific site (*FpS*). *FpG* is the standard ergodic approach of PSHA, where the site response is introduced by a period-dependent site correction factor that modifies the estimate of the considered GMPE. Such correction factors are built-in in practically all recent GMPEs (see e.g. the review by Douglas, 2011), either in terms of broad soil categories related to seismic norms, or of other engineering parameters such as Vs_{30}.

If, for a specific site, strong motion data are available at the site, the *FpG* approach can be refined (*FpS-1*), and the associated uncertainties possibly reduced, by application of a single-station sigma and the estimation of an empirically-based site-specific amplification factor ($\delta S2S$), as it will be extensively illustrated in this paper.

Finally, a further *FpS* approach may be followed (*FpS-2*), such as proposed by Bazzurro and Cornell (2004). This involves the convolution of PSHA results on outcropping bedrock by a conditional probability distributions of SAFs, i.e., of the site-specific ground motion amplification values at a specific vibration period, conditioned to the exceedance of a given level of ground motion at rock. This conditional probability distribution is generally estimated based on a wide set of parametric non-linear 1D wave propagation analyses, where the input accelerograms are scaled to encompass a wide level of amplitude levels of ground motions at outcropping bedrock.

In this study, we will refer to the *HyS* and the *FpS-1* approaches, that, for the reasons outlined in the sequel, allowed us to clearly identify and quantify the different sources of uncertainties in the site-specific PSHA results.

Objectives of this study

With the foregoing premises, the goals of this work are summarized as follows:

1. to compare the ground motion hazard estimates obtained from a data-based fully probabilistic non-ergodic one-step approach (*FpS-1*), that uses single-station site factors and sigmas derived from actual records, and from a hybrid site-specific two-step approach (*HyS*) that employs separate site response calculations;

2. to properly quantify the uncertainties related to both approaches, namely, within the *FpS-1* approach, those affecting the site factor and the site- and event-corrected residual, and, within the

HyS approach, those tied to the epistemic contributions related to different site-specific evaluations of the Vs profile, to the linear/non-linear soil models adopted in propagation analyses, to the seismic input in 1D calculations, and to the long-period 3D effects;

3. to show through application to specific sites how the different approaches under previous goal 1 can influence the actual SH assessment for the different representative return periods (RP) of 475 and 2475 yrs, of interest for building and other structures.

Region, sites and source model chosen for analysis

A densely inhabited and industrialized region of low-to-moderate seismicity, the Po Plain of Northern Italy, chosen herein as study area, is the central flat land in Figure 1. This also shows the historical and instrumental seismicity and a layout of a standard earthquake Area Sources (ASs) model for Italy, denoted ZS9 (Meletti et al. 2008), basis of the SH maps linked to the current Italian seismic code (NTC08), with some modifications introduced by Faccioli (2013). Readers should refer therein for the seismotectonic background (including active faults) and the input data for the SH analyses presented in the sequel.

Salient regional geo-tectonic elements pertinent to our study are illustrated in Figure 2. This highlights the surface projections of the fault ruptures of the damaging May 20 (M_w 6.1) and May 29 (M_w 6.0) 2012, Emilia mainshocks (Scognamiglio et al. 2012, Pezzo et al. 2013), the nearest accelerograph sites of the permanent and temporary RAN and INGV Italian networks (see Data and Resources Section), and the depth contours of bedrock proper, taken as the base of Pliocene. Most of the stations closest to the 2012 sources, and also to that of the 1996 M_w 5.4 Reggio Emilia earthquake (see Figure 2 for location), are aligned E-W, and some of them (notably MRN and T0821) lie above the top of buried ridges, as shown in Figure 2 (b), part of the larger Ferrara tectonic arc (see e. g. Lavecchia et al. 2012). MRN (Mirandola), T0821

(Casaglia) and NVL (Novellara) are considered as the main representative sites for the present analyses, typified in the upper 200 m or so by the two categories of *Vs* profiles shown in Figure 3. In the first category, which includes MRN and T0821**,** an impedance contrast occurs at 80-to-120 m depth, where the Late Messinian – Early Pliocene materials approach to the surface, with *Vs* in the 600-to-1000 m/s range. It will be seen that the three sites exhibit distinctly different values of the ground motion prediction residual parameters used in the non-ergodic hazard analyses illustrated in a later section.

For the earthquake source models, based on extensive previous work and sensitivity analyses (see Faccioli 2013), both a model-based seismicity representation and a gridded seismicity description were used. In the former, only the modified ZS9 AS model was introduced, with the seismic activity parameters listed in Appendix 1 (from Faccioli 2013, with slight modifications and updating). While fault models for hazard assessment in the region at study were discussed at length in Faccioli (cit.), they were not used herein. As a matter of fact, we checked that using a Fault Source + Background Activity representation and the single GMPE presently adopted led essentially the same uniform hazard spectra (UHS) as the AS model at NVL and MRN site, while at CAS the spectra derived from the AS model are more conservative.

Besides the AS model, a gridded seismicity representation has also been used in separate branches of the SH analysis, by applying a map of occurrence probabilities to a regular grid of point sources. Selected for this purpose was the time-independent, poissonian HAZGRID model (Akinci, 2010), in its latest version with CPTI11 (Rovida et al., 2011) as its reference catalogue for Italian earthquakes (updated with 2012 events). This model uses gridded historical seismicity that is spatially-smoothed to different length scales. The number of earthquakes with magnitude $M_w \geq M_{min} = 4.7$, in each cell “i” of the grid, is converted from cumulative to incremental values (i.e. number of events with magnitude M_w). For each cell of the grid (0.1° x 0.1°), the model estimates the G-R *a* and *b* parameters using the declustered catalogue. Gridded values of occurrence rates 10^a (earthquakes/cell/year) were computed and smoothed spatially by a two-dimensional Gaussian function with 25 km correlation length (Console and Murru, 2001).

Ground motion attenuation

The empirical attenuation models used in the present analyses were the regional ones developed by Bindi et al. (2011), herein ITA10, and its updated version ITA13, specifically developed by Pacor et al. (2013) within the SIGMA project (see Data and Resources section). ITA13 was derived from a Northern Italy dataset (called DBN2_B), the bulk of which comes from the 2012 Emilia seismic sequence, recorded by national accelerometer networks and temporary arrays installed after the 20 May 2012 mainshock.

The considered North Italy dataset features, among other things, relatively low spectral amplitudes at short periods, amplification of spectral ordinates in the distance range from 80 to 100 km (likely due to Moho reflections), and notable low-frequency amplification at stations lying on the Po Plain deep sediments. To capture these features, apart from the standard A, B and C site categories of Eurocode 8, an additional category, C1, was introduced that includes the stations on deep sediments within the Po Plain and, hence, should account for basin effects. The subsequent residual analysis by Pacor et al. (2014) (see Data and Resources section) shows that the site term is variable even for C1 sites, although these tend to have mostly similar geological features.

Since the North Italy dataset contains predominantly records from thrust fault events, mainly from category A and B sites at far distance and from C1 sites at short distance, we adopted the

ITA13 for source zones with predominant focal mechanism of thrust type; the study sites are all of the C1 category.

For shallow source zones with other styles of faulting, the ITA10 GMPE was adopted, following recommendations by Pacor et al. (2013). For ITA13 we have used the formulation with R_{jb} metric (Joyner and Boore distance), without conversion of M_L into M_w in the metadata, which provided the best score from LLH tests, see Pacor et al. (2013). For the passive subduction AS labelled SLAB in Figure 1, use was made of the Zhao et al. (2006) GMPE, version 'standard', option 'interface', in ergodic mode.

SH assessment via the one-step (non-ergodic) approach

One-step hazard estimation at study sites

We consider first the data-based direct hazard evaluation at the study, soil sites by a single-station sigma approach, skipping the intermediate bedrock ground motion determination.

We recapitulate here the following expressions for the single site, *s*, residual parameters from Rodríguez-Marek et al. (2011 and 2013), already referred to in the Introduction:

$$\delta S2S_s = \frac{1}{NE_s}\sum_{e=1}^{NE_s}\delta W_{es} \quad \text{(average site correction factor)} \quad (1a)$$

$$\phi_{ss,s} = \sqrt{\frac{\sum_{e=1}^{NE_s}\left(\delta W_{es} - \delta S2S_s\right)^2}{NE_S - 1}} \quad \text{(event and site-corrected single-station sigma)} \quad (1b)$$

$$\sigma_{ss,s} = \sqrt{\phi_{ss,s}^2 + \tau^2} \quad \text{(total single station sigma),} \quad (2)$$

where δW_{es} is the within-event component of the residual of the observed response spectrum ordinate with respect to the value predicted at site *s* for earthquake *e* via a GMPE, τ is the standard deviation of the between-event component of the same residual, and NE_s is the number of earthquakes recorded at site *s*. The term in parentheses in (1b), also denoted as δWS_{es}, represents the site- and event-corrected residual (Rodríguez-Marek et al. 2014), so that $\phi_{ss,s}$ represents its standard deviation.

Consistently with Rodríguez-Marek et al. (2014), the standard deviation, ϕ_{S2S}, of the site term $\delta S2S$ is not introduced in (2), to avoid double counting of its uncertainty if this term and its epistemic variability are reckoned with independently, as in the sequel. Essentially, we are estimating the median site intensity through the GMPE modified by $\delta S2S$, and the associated standard deviation through the single-station sigma (instead of the GMPE sigma).

The median spectral ordinate $Sa(T)$ is thus obtained by correcting the GMPE estimate as:

$$\mu_{corr\ Sa}(T) = \mu_{GMPE\ Sa}(T) \cdot 10^{\delta S2S(T)} \quad (3)$$

and the variability in $\delta S2S$ is handled as discussed in the sequel.

We used data from a set of 12 accelerometer stations with at least 10 earthquake records representative for deep soil deposits (see e.g. Figure 3), to estimate the standard deviation of $\delta S2S$ and $\phi_{ss,s}$ at the MRN, NVL, and T0821 study sites. (For CPC and MRN 9 records were actually available, and 8 for ISD; for the other stations, the number varies between 11 and 22.) In Figure 4 the high $\phi_{ss,s}$ values at NVL, as well as the anomalous de-amplification at T0821 may be noted.

The variability associated to $\delta S2S$ was assessed by computing the standard deviation ϕ_{S2S} from the 12-site sample in Figure 4 (left), and by deriving from it an independent estimate of the epistemic uncertainty in the mean value of $\delta S2S$, as

$$\sigma_{S2S,epistemic} = \frac{\phi_{S2S}}{\sqrt{N}} \quad (4)$$

with N = number of records at accelerometer site considered. Before applying (4), the standard deviation of $\delta S2S$ values for the 12-site sample and the whole 173-station sample used as a basis for ITA13 were compared. The ϕ_{S2S} for the larger sample is mostly between 0.20 and 0.25, while for the 12-site dataset $0.16 \leq \phi_{S2S} \leq 0.23$, showing that reliance on the 12-station subset is reasonable since the ϕ_{S2S} value derived from it is representative of the whole dataset, as well as of the deep Po Plain soil sites. Figure 5 (left), showing the site with corresponding $\pm 1\sigma_{S2S,epistemic}$ bands from (4) for MRN, NVL and T0821, makes it clear that the uncertainty we associate to the site factors is limited, notably at T0821; for the *N* values between about 10 and 20 at play in the three study sites, use of (4) leads to variations in amplification factors tied to $\sigma_{S2S,epistemic}$ of ±5% to ±15% with respect to the mean ($=10^{\delta S2S}$). Thus, the (epistemic) variability of $\delta S2S$ will be neglected in the sequel, considering the significantly larger variability carried by $\phi_{ss,s}$ into (2).

The single-station standard deviation $\sigma_{ss,s}$ is estimated through (1b) and (2) from the observations residuals at MRN, NVL and T0821 and deriving variability estimates for $\phi_{ss,s}$, while for the inter-event residuals the values of τ derived for the ITA13 GMPE are retained, which vary between 0.14 and 0.18 as shown in Figure 4 (left). Following Rodríguez-Marek et al. (2013), the epistemic uncertainty on $\phi_{ss,s}$ was estimated from its standard deviation across many stations (in this case the Po Plain 12-station set), thereby assuming implicitly ergodicity in the variance (not in the mean).

Stdev($\phi_{ss,s}$), i.e. the standard deviation of the event and site corrected single-station sigma values, has nearly constant values close to 0.08 for the large dataset and varies between 0.07 and 0.10 for the 12-station subset, while COV($\phi_{ss,s}$) is similar for the two datasets, so that using the value for the smaller subset as a measure of the variability of $\phi_{ss,s}$ looks justified. Inspection of the density distribution histograms of $\phi_{ss,s}$ of the 12-station subset at different periods indicates that the distributions tend to be non symmetric (consistently with the chi-square distribution that the uncertainty in the variance should follow), with the median lower than the mean and the single-site values for MRN and T0821 mostly close to the median.

Based on (2), the variability in $\phi_{ss,s}$ has been translated into an upper and a lower bound estimate of $\sigma_{ss,s}$ of the following form:

$$\sigma^{u}_{ss,s} = \sqrt{(\phi_{ss,s} + stdev\phi_{ss,s})^2 + \tau^2} \quad \text{and} \quad \sigma^{l}_{ss,s} = \sqrt{(\phi_{ss,s} - stdev\phi_{ss,s})^2 + \tau^2} \qquad (5)$$

Here, the $\phi_{ss,s}$ are those of the three study sites, stdev($\phi_{ss,s}$) is that of the Po Plain subset, and (as already stated) τ is the inter-event variability component of ITA13, neglecting its uncertainty. The foregoing variability estimates are illustrated in Figure 5 (right), which also shows that the ITA13 GMPE sigma represents a kind of average $\sigma_{ss,s}$ of the 3 sites. Note that introducing the variability bounds through $\phi_{ss,s}$ is intended to accommodate, at least in part, the uncertainty caused by multi-pathing, only partially accounted for in the available data owing to the predominance of the 2012 Emilia sequence records both at the study sites, and in the ITA13 GMPE.

The previous median and sigma formulations have been combined in a simple Logic Tree for SH estimation, shown in Figure 6. Apart from the two alternative formulations of earthquake source models, which effectively lead to markedly different hazard estimations, a salient aspect of the Logic Tree is that it features three branches to accommodate the variability of the single-site sigma, with an upper level branch, $\sigma_{ss,s}{}^{u}$, a mean level branch carrying the site-specific $\sigma_{ss,s}$ value, and a lower level branch $\sigma_{ss,s}{}^{l}$. These branches have been assigned weights that reflect in part the considerations previously made on the $\phi_{ss,s}$ density distributions for the 12-stations dataset. These led us to adopt the weights listed in Table 2.

The weights on the seismicity description in the Logic Tree were made to depend on the return period (RP), to account for the fact that the gridded seismicity representation reflects basically the earthquake catalogue, regarded as reliable (for the higher magnitudes) over a time span not exceeding 500 to 1000 years. Thus, for the 2475-yr a significantly smaller weight was assigned to this representation.

PSHA calculations were performed with the CRISIS2008 code, in its latest version, 2014 (see Data and Resources Section), using ITA13 GMPE in partially nonergodic mode only for the ASs associated in ZS9 (Meletti et al., 2008) to predominant reverse faulting, namely (referring to Figure 1) 905, 906, 907, 910, and SPP. The ITA10 GMPE (in ergodic mode) was instead associated to all other shallow ASs with predominantly normal and strike-slip faulting, while the Zhao et al. (2006) GMPE, in version 'standard', with interface option, ergodic, was used for the subduction-like SLAB AS (see Figure 1).

Perusal of the hazard curves has shown that the contribution of the SLAB AS is dominant-to-high only at T0821, and medium-to-low at the other two sites. ASs 915 and 916 give a high contribution only at long period at all three sites, while the influence of SPP dominates at MRN and NVL, but decreases at T0821.

Figure 7 illustrates the UHS at two of the selected sites, stemming from both the AS model and the gridded source model, with the mean, upper and lower level estimates of the spectra yielded by the individual Logic Tree branches in Figure 6. Shown in Figure 7 are also the current code spectra (Norme Tecniche per le Costruzioni, NTC2008), as well as the spectra from the records of significant recent earthquakes, i. e. the 1996 (M_w 5.4) Reggio Emilia event, recorded at NVL, and the Emilia 2012, May 29th (M_w 6.0) mainshock, at MRN, see Figure 2. Note that the observed spectra are mostly within the spread spanned by the Logic Tree branches for 475 yrs RP and that the spectral shapes are reasonably similar. The code spectra are consistent with the

UHS at 475 years. The AS model is generally more conservative than the gridded model at MRN and T0821 (not shown), but not at NVL.

The results from the Logic Tree calculations for the three studied sites, with the weights shown in Table 2 are displayed in Figure 8 as percentile-level UHS.

To be noted in Figure 8 are: the large (84-16) percentile spread at NVL compared to T0821 and MRN, consistent with the high $\sigma_{ss,s}$ shown in Figure 5 (right), and the anomalous low spectral levels at T0821, the interpretation of which remains uncertain (possibly depending on source-to site propagation effects).

Direct hazard estimation on exposed bedrock

Hazard estimation on exposed bedrock, required in a two-stage PSHA, followed the same general logic described in 4.1, with the essential difference that bedrock records were not available (as in most cases) for direct evaluation of $\phi_{ss,s}$ and $\delta S2S$. At the study sites, as in the Po Plain at large, the upper sediments are from about 100 m to many hundreds of m thick and, with a partial exception, there are no borehole records within hard, geologically older formations to rely on. (Data from in-hole instruments are as a matter of fact available at a site located some 500 m S of T0821 (Margheriti et al. 2000), but only of weak motions from distant or low-magnitude events, that were not considered suitable for this study.)

In dealing with bedrock motions, we disregarded the influence of κ, the near-site attenuation factor causing an $\exp(-\pi\kappa f)$ type high-frequency decay in the Fourier spectrum amplitude, and the associated uncertainties. Actually, two out of three study sites, i.e., MRN and T0821, belong to a subsoil profile family of the Po Plain where hard formations with Vs of about 800 m/s are encountered at around 100 m depth (see Figure 3), with a marked impedance contrast with the upper sediments. For ITA13, as well as for several other GMPEs $V_{s30} \geq 800$ m/s characterizes standard rock, i.e., ground type A of Eurocode 8 (CEN, 2003), corresponding to type B of NEHRP criteria (BSSC, 2003).

Regionally based $\delta S2S$ values applicable on exposed rock and their dispersion were assessed starting from two different data subsets from accelerometer sites on ground type A from the ITA13 dataset, i.e., those within 120 km distance from the main events of the Emilia 2012 sequence (large grey circle in Figure 9, left), and those within 75 km radius in Figure 9 (dark, smaller circle, left). Restricting further the selection to sites with at least 5 records yielded subsets of 21 and 4 sites, respectively. The mean $\delta S2S$ from the two subsets are rather close at long period, but at short period those for the smaller group are biased towards negative values due to the records of the strong thrust fault events of May 2012, that generated lower amplitude motion at the southern stations with respect to those to the North like MLC and TGG in Figure 9, right (see Luzi et al. 2013). Thus, only the larger subset was retained, with the results shown in the right graph in Figure 9.

The mean regional value of δS2S on rock, inferred from Figure 9, is very close to zero, suggesting lack of bias from the dataset used, while the standard deviation ϕ_{S2S} is largest at short period (0.35) and almost constant around 0.17 for $T > 0.35$ s. These values are nearly the same as for the whole ITA13 dataset. Furthermore, since for the < 120 km dataset there is an average N_{av} = 12 records per site, use of (4) leads to a gross estimate of $\sigma_{S2S\ epistemic}$ on rock, ranging between 0.10 at short period and 0.05 for $T > 0.35$ s. As for soil sites, and for the same reasons, we neglect this uncertainty in the sequel and use uniformly $\delta S2S = 0$ for exposed bedrock in (3).

For the ϕ_{ss} regional value, analysis on the 120 km dataset yielded the mean $\pm 1\sigma$ range depicted on the left of Figure 10 where the close agreement of the mean with the Rodríguez-Marek et al. (2013) “constant model” will be noted, with only a slight divergence at long period. Inspection of the distribution hystograms of ϕ_{ss} revealed a non symmetric behaviour, with median values mostly below the mean at short period.

By taking again the upper and lower bounds of (5) for the variability range associated to the regional mean single-station σ_{ss}, as well as the value of τ of the ITA13 GMPE, the result shown on the right of Figure 10 was obtained, i.e., a range for σ_{ss} that lies entirely below the standard deviation associated to the ITA13 GMPE. This result, when compared with that shown on the right of Figure 5, points to a substantial difference between the Po Plain soil sites and the nearest surrounding rock sites in terms of prediction variability. The Logic Tree of Figure 6 was again used for the PSHA on rock at the study sites; to reflect the noted non-symmetric distribution of $\phi_{ss,s}$ values, notably at short period, the weights shown in last column of Table 2 were assigned to the three study sites.

The results of the PSHA on exposed type A ground are displayed in Figure 11; the non-ergodic UHS, all calculated with $\delta_{S2S} = 0$ and with an average σ_{ss} significantly lower than the GMPE sigma, are all reasonably consistent with the code spectra at 2475 yrs and somewhat on the low side for 475 yrs. As expected, the UHS show lower amplitudes with respect to ground type C spectra shown in Figure 8, except for the T0821 site. Ground type A and C spectra for T0821 show similar values, due to the selected site specific $\delta S2S$ and σ_{ss} used in the one-step analysis.

Evaluating site-specific probabilistic response spectra and associated uncertainty in the hybrid, two-step approach: the case of Mirandola

Selected approach for site-specific PSHA

With the aim to identify and quantify the different sources of uncertainties in site-specific PSHA studies based on 1D seismic wave propagation analyses, we limited ourselves to using a *HyS* approach, according to the following steps:

1. the mean UHS on exposed bedrock is considered as a target for input motion selection at a a specific return period;
2. real accelerograms are selected, with response spectra approaching as closely as possible the target spectrum in a broadband sense, i.e., from 0 to 5 s period;
3. the selected accelerograms are then subjected to an iterative amplitude scaling in the frequency domain, with no phase variation, until matching with the target spectrum is achieved;
4. 1D site-specific propagation studies are carried out with the input motions at the previous step, considering the sources of epistemic uncertainties in the modelling assumptions, as discussed in the sequel.

In the framework of our study, using this procedure is justified based on the following considerations. First, the broadband compatibility with the target UHS of the selected (unscaled) time histories ensures that, even after scaling to the target spectrum, the features of the accelerogram related to the seismic source properties, especially in the long period range, are basically preserved, as discussed by Smerzini et al., 2014. This can be accomplished by making use of a high-quality dataset, containing only digital recordings of engineering relevance, obtained at close distance ($R < 30$ km) from moderate to large magnitude earthquakes ($5 < M < 7.5$). Figure 12 shows a sample result of such iterative frequency-scaling procedure, pinpointing the consistency of original and corrected records, especially in the long period range. Second, no additional aleatory variability is introduced in terms of spectral ordinates of input motion, thus avoiding any double counting problem. Note that a further unavoidable contribution to aleatory variability is due to the non-unique correspondence of acceleration time history and response spectrum, so that an infinite number of acceleration time histories may correspond to the same response spectrum. As will be shown later, this contribution may be significantly reduced by the spectral matching procedure outlined before.

Third, having selected the input motions to match the UHS for the selected return period, makes the resulting site amplification functions consistent with the desired hazard level. Note that our objective is more restricted than that of the *FpS* approach of Bazzurro and Cornell (2004), where the full surface-hazard curves are derived from the rock-hazard curves through a convolution integral with the conditional amplification function probability distribution. This integral allows one to combine also (frequent) low intensity bedrock motions with the high (and improbable) amplification function that would result from sampling the tails of the amplification function distribution. However, the practical application of the Bazzurro and Cornell approach is entirely based on 1D numerical site response calculations, probably unfit to handle the tails of the amplification functions, which should be more properly dealt with by more complex approaches. Moreover, the approach in question lacks observational validation of the conditional distributions with data from well instrumented sites, e. g. from the Kik_net.

Finally, we are able in this way to clearly disaggregate and identify the role of the different factors contributing to the overall epistemic uncertainty in the site-specific PSHA results, such as illustrated in the sequel.

Evaluation of sources of uncertainty in site-specific seismic response analyses

For a given target spectrum on rock, the sources of uncertainties in site effects evaluation can be identified as related to (see e.g., Rathje et al., 2010): (a) selection of input motions; (b) dynamic properties of soil profile; (c) selection of the method of analysis for site effects evaluation; (d) modeling of non-linear soil behavior. To avoid double counting of aleatory uncertainties, only epistemic contributions will be referred to in the following, so that the small scale random variability of soil properties is disregarded. As a matter of fact, we considered that the impact of the small scale random variability in the mechanical properties of the propagation path already enters into the ϕ_{ss} uncertainty component of the partially non ergodic analysis, by which the bedrock UHS were determined.

Although these sources of uncertainties are in principle correlated (e.g., the effect of a specific assumption for the non-linear soil model is generally amplified by the way input motion is selected), we will treat them as independent contributions, to quantify the relative impact of each component for the case under study.

More specifically, taking as a target the Mirandola (MRN) site considered in the previous sections, the following contributions to the overall uncertainty are explored:

- linear-elastic soil models in terms of *Vs* profile;
- non-linear *G* vs. γ (=cyclic shear strain amplitude) and damping ratio ξ vs. γ curves;
- non-linear modelling method.

Only 1D soil models under vertically propagating waves are considered herein, the analysis of more complex models, such as 3D in the near-source range, being currently under way. The 1D propagation analyses have been performed according to three different approaches, namely, linear visco-elastic (LIN), equivalent-linear (EQL) and fully non-linear (NL), using in all cases the DEEPSOIL code (see Data and Resources Section).

The Mirandola site

We have focused our attention on one of the three previous study sites, MRN, that, owing to its location in the epicentral area of the May 2012 Po Plain seismic sequence, was carefully investigated under different projects. After the seismic sequence, various site investigations were carried out for seismic site characterization in the area most heavily affected by the earthquakes (see Data and Resources section). One of the most interesting results is that the *Vs* profile spatial variability is rather limited, as shown by the plot in Figure 13, referring to sites in the Mirandola urban area, at minimum relative distance of few hundreds m. The *Vs* coefficient of variation, at least down to about 100-120 m where the engineering bedrock is found, is around 10-15%.

Selection of input motions

As stated previously, we used an iterative procedure in the frequency domain to scale, in a broad frequency range, a set of carefully selected real records to the target UHS on exposed bedrock for the return periods RP = 475 yrs and RP = 2475 yrs. These two sets, listed in Table 3, were used as excitation for the subsequent wave propagation analyses. The time histories of two of such records have been plotted in Figure 12, both in the original and scaled versions. The average Magnitude and epicentral distance of the selected records are M_w = 5.9 and R_{epi}=21 km for RP = 475 yrs, and M_w = 6.4 and R_{epi}=18 km, respectively, which are reasonably close to results of PSHA disaggregation at MRN site for an intermediate period of 1 s. Furthermore, all these records were selected on either EC8 A or B site classes.

Effect of epistemic uncertainties of the *Vs* profile

We have considered the *Vs* profiles in Figure 13 and assumed that differences of such profiles represent the epistemic uncertainty in the selection of the model for 1D analyses. Indeed, the profiles come either from different techniques or from nearby locations, so that selection of any of them should be considered as a possible modelling choice.

We have first quantified the variability introduced by the *Vs* profile uncertainty by considering the following combinations, for each return period: a) an unscaled set of input motions, with average response spectrum that approaches within a small tolerance the target spectrum; b) scaled motions, with spectral matching limited to the 0-1 s period range and, c) scaled motions, but with broadband spectral matching (up to 5 s). The results are shown in Figure 14, on the left hand side in terms of average surface response spectra and, on the right hand side, in terms of standard deviation sigma of the corresponding spectral ordinates. For simplicity, we show here only results from the equivalent-linear approach. Note that, for the original set of unscaled records, the resulting average spectrum is slightly lower, because such spectrum did not exactly match the target UHS. However, the sigma is much higher than for the scaled accelerograms. Also, when the spectral match is band-limited, e.g., in the 0-1 s range, the dispersion in the output response spectra increases sharply as soon as one looks at periods far from the range selected for matching. Therefore, application of spectrally matched records is found to reduce significantly the variability of output response, in this case by a factor of around 3, depending on how close the unscaled record approaches the target spectrum. Of course, in this way the influence of the aleatory uncertainty of multiple response spectral shape of the input motions is disregarded, in line with our objective to quantify only the epistemic uncertainty contributions.

The results shown in Figure 14 combine the effects of different *Vs* profiles and of different input motions. However, we have verified that the resulting variability, when broadband spectral matching is considered, is dominated by the *Vs* profile uncertainty, while the contribution of input motion is minor. Note that, since input motions are scaled to match the target spectrum, the latter contribution is to be attributed to the aleatory variability of different acceleration time histories having the same spectral ordinates.

Influence of the soil modelling assumptions on the non-linear soil response

Four types of curves representing G/G_{max} and damping ratio ξ vs shear strain amplitude γ were investigated herein, i.e.: (i) Darendeli (2001); (ii) Ishibashi and Zhang (1993); (iii) the mean standard curves of Seed and Idriss (Upper Limit) independent of confining pressure (Seed and

Idriss 1970; Idriss 1990; Seed et al., 1986), and (iv) Resonant Column (RC) test results obtained on undisturbed samples of clay and sand extracted from different depths at a few Po Plain sites, at some distance from Mirandola. More specifically, the clay samples were obtained at the site of San Carlo (at depths from 2 to 12 m), and the sand samples at the sites of Canale Boicelli and Po di Volano (at depths of about 40 m), at 42 and 70 km from MRN, respectively (from Fioravante and Giretti, 2013, in Data and Resources section). Note that for cases (i) and (ii), curves depend on the mean effective confining stress σ'_m, while for cases (iii) and (iv) such dependence is disregarded.

The resulting curves are compared for two representative depths in Figure 15, while the detailed description of the selected *Vs* profile used for these analyses is shown in Table 4.

Using the foregoing soil profile, and the nonlinear soil curves shown above, both equivalent linear and non-linear analyses were performed with the DEEPSOIL code (see Data and Resources Section).

The computed response spectra at ground surface are shown in Figure 16 for the two RPs of 475 and 2475 years, respectively, and show that differences in average spectral values of equivalent-linear vs fully non-linear approaches are in this case limited, and mostly in the short period range, around 0.1 s. The quantification of the resulting variability according to the three different selected approaches (LIN, EQL, NL) is summarized in Table 5 for different period ranges and the two RPs under study.

Note that the variability due to the soil modelling assumption (denoted by σ_{soil_model} in Table 5) is larger than that due to the *Vs* profile (σ_{Vs} in Table 5), and, as expected, it tends to increase with increasing RP and tends to vanish at long periods, provided that input data is spectrally matched with target. This tendency is typical for 1D wave propagation analyses but, as it will be commented later, provides unrealistically low values when compared to observed variability of spectral amplification functions at long periods from Kik-net records (see Data and Resources section).

Is the soil response at MRN non-linear?

In this work, the previous LIN, EQL and NL approaches for 1D wave propagation have been considered separately. In the framework of a logic-tree approach, a weight should have been assigned to each of these assumptions, based on the best in-situ data available and engineering judgement. However, we preferred to avoid such a Logic Tree -based approach at this stage, and tried to exploit as far as possible the evidences coming both from records of the Emilia 2012 sequence and from similar deep soil sites of the Kik-net.

For this purpose, we first illustrate in Figure 17 a summary of results from the site-specific PSHA at the MRN site, namely, from the non-ergodic approach and from the two-step hybrid approach involving alternatively the LIN, EQL and NL approaches (in the latter cases, the Fioravante model was considered). For reference, the records at MRN during the two mainshocks of May 20 and 29, 2012, are also shown in the same figure.

It is clear that the LIN approach yields short-period spectral accelerations much larger than those from non-linear simulations, either from the EQL or NL approaches. However, if we consider in Figure 17 the result of the one-step seismic hazard analysis, we can deduce that the soil/rock amplification functions, implicit in the one step PSHA approach, are in reasonably good agreement with the LIN analyses, while they exceed by far the prediction by non-linear models.

Thus, is non-linear soil response an issue for the MRN site? Although this puzzling question will be the subject of further research, there are some additional hints, together with the results in

Figure 17, suggesting that the standard non-linear soil response analyses may strongly underestimate the actual surface ground motion levels.

First, the PGA levels recorded at MRN during the May 20 and May 29 earthquakes, both $M_w \sim 6$, reach 0.3 g in the horizontal direction, up to an impressive 0.9 g in the vertical direction: such values are hardly compatible with significant non-linear effects at deep soil sites. As shown in Figure 17, the observed value of 0.3 g is not even approached for RP = 2475 yrs, which is much larger than the estimated recurrence time of the seismic event on the Mirandola fault (about 800 yrs according to Pezzo et al., 2013).

Second, a pervasive lack of evidence of significant non-linear response at deep soil sites, without significant pore pressure earthquake induced build-up, also comes from the analysis of a total of 21 stations of the Japanese Kik-net, selected considering deep soil sites with similar *Vs* as in the Po Plain (Paolucci et al., 2014, see Data and Resources section). One of the most meaningful examples is the NIGH11 station, which recorded about 100 events, 7 of which with *M* ranging from 6 to 7 and epicentral distance from 10 to 30 km. Shear-wave velocity at this site ranges from about 400 m/s to about 650 m/s at 200 m depth. In Figure 18 the response spectral amplification functions (SAFs), measured by the ratio of the spectral ordinates at ground surface and at the borehole sensor for a set of periods, are plotted as a function of the amplitude of motion at the borehole sensor, measured by the pseudo-spectral velocity at the corresponding period. These ratios are almost constant, independent of the amplitude of motion at the borehole site, suggesting that no significant non-linear effect has influenced ground response. Referring to Paolucci et al. (2014) for a more general discussion of results for deep soil sites in the Kik-net, the following remarks can be made:

- Spectral Amplification Functions (SAFs) at considered deep soil sites in the Kik-net do not show a significant dependence on the intensity of motion at bedrock, suggesting no clear evidence of non-linearity, despite the relatively soft soil conditions;
- The observed variability of SAFs at Kik-net deep soil sites is generally limited, in spite of the wide range of magnitude and distances encompassed by records. σ_{log10} ranges typically between 0.04 and 0.08 (σ_{ln} from 0.09 to 0.18); furthermore, no clear evidence is found of a dependence of σ_{log10} on period, while, based on 1D site response analyses, a significant reduction of variability would be obtained for increasing periods.

Combining the epistemic contributions to total σ

The combination of different epistemic contributions to σ from 1D analyses is made according to the following rule (see Table 5):

$$\sigma_{epistemic\_1D} = \sqrt{\sigma_{Vs}^2 + \sigma_{\text{soil\_model}}^2}$$

where σ_{Vs} includes the effect of different Vs profiles ($\equiv\sigma_{1D\_epistemic}$ for the LIN case) and σ_{soil_model} includes the effect of different non-linear soil models (G-γ and ξ-γ curves). As pointed out previously, all contributions include the combined effect of variability of input motion, found to be negligible.

In the first row of the same Table, we have also introduced as a reference the $\sigma_{Kik\text{-}net}$ values computed from the SAFs of the 21 deep soil sites considered from the Kik-net, mentioned in the previous section. Although the latter values of σ are in general related to the combination of a wider set of seismic site amplification factors, rather than 1D effects alone, they can reasonably be considered as a lower bound for evaluations of site-specific variability of results.

Therefore, the resulting σ_{TOT} associated to the average site-specific response spectra for a given return period, including both the epistemic uncertainties of the site response analysis and the total (aleatory+epistemic) uncertainties carried by the PSHA at exposed bedrock (σ_{PSHA_rock}) can be evaluated as:

$$\sigma_{TOT} = \max_{T}\left(\sqrt{\sigma^{2}_{epistemic\_1D} + \sigma^{2}_{PSHA\_rock}}\,;\sigma_{Kik-net}\right)$$

As a summary, Figure 19 compares results from all the analyses performed for the MRN site, i. e. PSHA one-step analyses (black lines), and the two-step hybrid approach analyses. The latter involved both LIN 1D wave propagation calculations, performed with the 7 corrected acceleration records and the 7 available profiles, dark grey lines, and the corresponding NL calculations, with the soil models discussed in Section "Influence of the soil modelling assumptions on the non-linear soil response" (light grey lines). The associated sigma values are the σ_{TOT} (LIN and NL) discussed in the previous section and listed in Table 5, while the σ_{TOT} values for the one-step analysis range from about 0.09 at short periods to about 0.06 at long periods. For simplicity, results from EQL approach are not shown, being similar to the corresponding NL results, see Figure 17.

As previously discussed, the agreement between the one-step and the two-step approach is satisfactory only if the LIN assumption holds for soil response at MRN. As expected, this assumption plays a growing role with increasing return period and, for RP = 2475 yrs, a sharp disagreement exists between the NL predicted spectrum and that obtained both by the LIN approach and the one-step UHS. The better agreement with the LIN two-step results may also be related to the fact that in the one-step approach δS2S is assumed to be a constant, which is the same as saying that it is linear. To remove the constant δS2S assumption implies making this term dependent on a measure of the shaking intensity so that the correction factor $10^{\delta S2S}$ in (3) would account for such non-linearity; this is a task beyond the scope of our work

Discussion

Through the use of the residual measures of spectral response predictions, yielded by a GMPE expressly developed for Northern Italy, we first carried out a single-site sigma, one-step PSHA (type *FpS-1* in Table1) at three accelerometer sites lying on the deep sedimentary deposits of the Po Plain, expected to generate 3D basin-type propagation effects. Residual measure uncertainties were estimated from the variability assessed on an appropriate subset of the regional dataset. Although the study sites all belong to the same subsoil profile category, and share the same broad geological conditions, their site terms were found to sharply differ both at short and long periods, showing de-amplification with respect to the average GMPE prediction (at two different levels) at all periods in two cases (T0821 and NVL) and moderate amplification in another (MRN). Significant differences were also observed in the site- and event-corrected residual variability $\phi_{ss,s}$, leading to markedly different single-site sigmas in two cases out of three, with the lowest sigma (well below the ergodic sigma of the regional GMPE) at the de-amplifying T0821 site. 3D effects linked to seismic ray defocusing are possibly responsible, at least in part, for the anomalous behavior observed at T0821 and for the ensuing hazard levels predicted therein, with UH spectra way below those of the other two sites, as well as of the seismic code spectra. The results suggest associations between response spectrum prediction residuals and local geological setting that may be difficult to interpret, due to likely 3D propagation effects at specific sites and, possibly, also to rupturing earthquake faults at close range. Thus, while the mean ϕ_{ss} from a Po Plain deep sediments dataset matches those from other regional datasets

(Rodríguez-Marek et al. 2013), importing the variability of the latter into a single-site sigma PSHA at some of the sites we analyzed, e.g. T0821, could be inconsistent.

The records from the damaging 2012 Emilia earthquake sequence ($4.0 \leq M_w \leq 6.0$) predominate in the regional dataset presently used and, moreover, many data of that sequence were recorded by temporary stations whose location was dictated by the epicenter locations, as suggested by the predominant EW alignment in Figure 2. Actually, only the NVL station has recorded at close distance significant events other than those of 2012, and with different azimuth. However, while variability due to multi-pathing is underrepresented in our hazard estimates, the data and the residual parameters we used reflect well the influence of the potentially most hazardous sources for the analyzed sites, notably for MRN (lying in the very near field of the May 29, 2012 shock) at short and intermediate period. At long periods the variability estimated from a set of sites seems reasonably conservative (see right graph of Figure 5). The (84-16) percentile spreads of the UHS spectra differ by up to nearly a factor of five at the three study sites, a warning on how sensitive the uncertainty estimates can be to the local geology and to the source factors.

A similar approach was followed to estimate single-site sigma UHS on exposed bedrock at the same locations, but the absence of records from borehole instruments induced us to recur to regionally based estimates of site-term and site-and-event-corrected variability. As in the case of the surface soil sites, the site term variability on rock was considered small in comparison to the other and was neglected. No site term was used this time in the PSHA because a sizable regional subset of 21 rock sites exhibits a nearly vanishing mean of such term at all periods. The mean ϕ_{ss} from the same subset was found to be closely consistent with that of Rodríguez-Marek (2013) constant model, and to give rise to a mean single-site sigma on rock significantly lower than that of individual soil sites and, especially, of the ergodic sigma of the regional GMPE, a difference causing the single-site sigma rock spectra to lie markedly below their ergodic counterparts.

Based on the UHS at bedrock for two return periods, i.e., RP = 475yrs and 2475 yrs, we computed the corresponding site-specific response spectra at the MRN site with the main objective to quantify the effect of different sources of epistemic uncertainty in the site response evaluation at a deep soil site and to combine them into a single measure of uncertainty including both contributions from PSHA at exposed bedrock and from site response evaluations.

A thorough approach was devised for this purpose, allowing to remove from the analysis the aleatory sources of uncertainty, already accounted for in the PSHA on rock. In this respect, a key role was played by the criterion by which the input motions for 1D site response evaluations were selected. We found that the following recipe is suitable for preserving as far as possible the physical nature of the records and, at the same time, for avoiding double counting of aleatory variability: (i) carefully select real records approaching as closely as possible the target spectrum in a broadband sense (e.g., from 0 to 5 s period) and (ii) iteratively scale the amplitude of such records in the frequency range, with no phase change, to match closely the target spectrum.

The epistemic contributions in the 1D modelling phase were subsequently evaluated separately for the different LIN, EQL and NL approaches considered, finding that the assumptions on the G-γ and ξ-γ curves dominate the resulting variability of results, for both EQL and NL approaches, especially for large return periods.

We are convinced that managing the uncertainties in the site specific response analyses within the HyS approach (see Table 1), should not follow a logic-tree philosophy. Rather, the best in-situ data available should drive the engineering judgment towards a single and neat decision, without recurring to an average of different weighted branches. For this reason, after considering separately the different approaches to 1D modelling, we concluded that the LIN approach provided the best results for the MRN site. Although exploring in detail this important subject is beyond the scope of this paper, this conclusion was based on various hints, specifically: (i) the similarity of the one-step UHS at MRN resulting from non-ergodic single site PSHA with the two-step result based on the LIN approach; (ii) the comparison with observed records at MRN during the mainshocks of the 2012 seismic sequence, showing PGA and short period spectral levels well beyond those predicted based on different non-linear assumptions; (iii) a similar evidence from a set of 21 stations at deep soil sites of the Japanese Kik-net.

We finally note that in this work we have benefitted from a wealth of site-specific strong motion records. For sites for which PSHA is required, where no such records are available either at the local or at the regional level, we recommend to have recourse to the Rodriguez – Marek et al. (2013) constant model for the event corrected single-station sigma (ϕ_{ss}) and to the between-event component (τ) of the standard deviation of regionally applicable GMPEs for the corresponding residual component in (2). In this case, the site term ($\delta S2S$) in (3) should be taken equal to zero, and a hybrid approach (HyS) with site-specific response analysis should be performed.

Data and Resources

Station data (including soil profiles) and records of the RAN (http://itaca.mi.ingv.it/ItacaNet) and INGV (http://ismd.mi.ingv.it/ismd.php) Italian accelerometer networks, as well as ITACA database (http://itaca.mi.ingv.it; Pacor et al., 2011), have been used for the three analyzed sites of NVL and MRN (RAN permanent stations), and T0821 (INGV temporary station).

Ground motion attenuation models and corresponding residual measures extensively used in this work come from the following SIGMA project (http://projet-sigma.com/organisation.html) documents: Pacor F., L. Luzi, R. Puglia, and M. D’Amico (2013). Calibration of GMPEs for Po

Plain region. Deliverable D2-72; and Pacor F., G. Lanzano, M. D’Amico, C. Felicetta, L. Luzi and R. Puglia (2014). Ground motion variability in the Po Plain region, Deliverable D2-133. Within the same project, the authors had developed a preliminary formulation of their present results on site-specific PSHA in: Paolucci, R., E. Faccioli, C. Smerzini, and M. Vanini (2014). Approaches to account for site effects in the PSHA of selected sites in the Po Plain area. Deliverable D3-96 of Project SIGMA.

This work also relied on previous work carried on by the authors within an Italian National Project funded in the frame of DPC-INGV Agreements (the 3rd S2 Project, 2012-2013, concerning the mid-long term SHA in Italy and focusing in two priority areas, one of which was the Po Plain and the sites of MRN and T0821). See: Progetto S2 (2012). Site-specific hazard assessment in priority areas. Deliverable D4.1, INGV-DPC S2 project (https://sites.google.com/site/ingvdpc2012progettos2/). Soil profiles and results from Resonant Column (RC) test obtained within this Project have been used.

Results from RC tests on sand samples at the sites of Canale Boicelli and Po di Volano come from Fioravante, V. and D. Giretti D. (2013). Schede di caratterizzazione geotecnica dei principali litotipi. In L. Martelli and M. Romani (eds): Microzonazione Sismica e analisi della condizione limite per l’emergenze delle aree epicentrali dei terremoti della Pianura Emiliana di Maggio-Giugno 2012. Available online at: http://mappegis.regione.emilia-romagna.it/gstatico/documenti/ord70_20121113/Allegato_1_6_schede_caratterizzazione_geotecnica.pdf.

Soil profiles used for comparison have been borrowed from Albarello, D., D. Pileggi, and F. Guerrini (2011). Misure di vibrazioni ambientali a stazione singola ed antenna, Technical Report for “Verifiche sismiche delle opere idrauliche, Argini del fiume Po”, Parma, April 12, 2011, available at http://www.adbpo.it.

Data from the Japanese Kik-net database (http://www.kyoshin.bosai.go.jp/) have been extensively used in this work.

PSHA analyses were performed using software CRISIS, in its 2014 version. (see: Ordaz, M., Martinelli, F., Aguilar, A., Arboleda, J., Meletti, C., and D’Amico, V. (2014). Crisis 2014 user manual (software help). Technical report, II-UNAM; and Ordaz, M., F. Martinelli, V. D’Amico, and C. Meletti (2013). Crisis2008: a flexible tool to perform probabilistic seismic hazard assessment, *Seism. Res. Lett.* **84**, 495–504.)

For site response analyses the DEEPSOIL software was used, available online at www.illinois.edu/~deepsoil. See: Hashash, Y.M.A, D. R. Groholski, C. A. Phillips, D. Park, and M. Musgrove (2012) “DEEPSOIL 5.1, User Manual and Tutorial.” 107 pp.

All other data used in this article come from published sources listed in the references.

Acknowledgements

This research, partly funded by ENEL, Italy, under contract n. 1400054350, was conducted in the framework of the international SIGMA Project (Research and Development Programme on Seismic Ground Motion). Interaction within the Project with M. Corigliano and R. Figini (ENEL), and with P. Burrato, F. Pacor and G. Valensise (INGV) is gratefully acknowledged. Authors express their gratitude to the Japanese Research Institute for Earth Science and Disaster Prevention (NIED) for making the KiK-net Strong Motion records available.

We acknowledge Aybige Akinci who has performed the calculations to update the HAZGRID model up to 2012 Emilia earthquake sequence.

References

Akinci, A. (2010). HAZGRIDX: earthquake forecasting model for ML ≥ 5.0 earthquakes in Italy based on spatially smoothed seismicity, *Ann. Geophys.*, **53**(3), 51-61.

Al Atik, L., N. A. Abrahamson, J. J. Bommer, F. Scherbaum, F. Cotton, and N. Kuehn (2010). The variability of ground-motion prediction models and its components, *Seismol. Res. Lett.* **81**(5), 794–801.

Bazzurro, P. and Cornell, C.A. (2004a). Ground-motion amplification in nonlinear soil sites with uncertain properties, *Bull. Seismol. Soc. Am.* **94**, 2090-2109.

Bazzurro, P. and Cornell, C.A. (2004b). Ground-motion amplification in nonlinear soil sites with uncertain properties, *Bull. Seismol. Soc. Am*. **94**, 2110-2123.

Bigi, G., G. Bonardi, R. Catalano, D. Cosentino, F. Lentini, M. Parotto, R. Sartori, P. Scandone and E. Turco (Eds.) (1992), Structural Model of Italy 1:500,000. CNR Progetto Finalizzato Geodinamica.

Bindi, D., F. Pacor, L. Luzi, R. Puglia, M. Massa, G. Ameri, and R. Paolucci (2011). Ground motion prediction equations derived from the Italian strong motion database, *Bull. Earthq. Eng*. **9**, 1899–1920.

Boccaletti M., G. Corti, and L. Martelli (2010). Recent and active tectonics of the external zone of the Northern Apennines (Italy), *Int. J. Earth Sci.* **100**, 1331-1348.

BSSC, Building Seismic Safety Council (2003) The 2003 NEHRP recommended provisions for new buildings and other structures. Part 1: Provisions (FEMA 450). Available online at www.bssconline.org

CEN, European Committee for Standardization (2003). Eurocode 8: design of structures for earthquake resistance. Part 1: general rules, seismic actions and rules for buildings, Bruxelles.

Chen, L. and E. Faccioli (2013). Single-station standard deviation analysis of 2010–2012 strong-motion data from the Canterbury region, New Zealand, *Bull. Earthq. Eng*. **11**, 1617−1632.

Console, R., M. Murru, G. Falcone, and F. Catalli (2008). Stress interaction effect on the occurrence probability of characteristic earthquakes in Central Apennines. *J. Geophys. Res.* **113**, B08313, doi:10.1029/2007JB005418.

Cramer C. H. (2003). Site seismic-hazard analysis that is completely probabilistic, *Bull. Seismol. Soc. Am.* **93**(4), 1841–1846.

Darendeli, M. B. (2001). “Development of a new family of normalized modulus reduction and material damping curves.” PhD dissertation, Univ. of Texas at Austin, Texas.

Douglas J. (2011). Ground-motion prediction equations - 1964-2010. Technical Report published jointly by Pacific Earthquake Engineering Research Center (PEER) and by Bureau de Recherches Géologiques et Minières (BRGM), BRGM/RP-59356-FR. Available online at peer.berkeley.edu.

Faccioli, E. (2013). Recent evolution and challenges in the Seismic Hazard Analysis of the Po Plain region, Northern Italy. The second Prof. Nicholas Ambraseys distinguished lecture, *Bull Earthq. Eng*. **11**, 5–33.

Ishibashi, I., and X. J. Zhang (1993). Unified dynamic shear moduli and damping ratios of sand and clay, Soils Found. **33**(1), 182–191.

Lavecchia G., R. de Nardis, D. Cirillo, F. Brozzetti, P. Boncio (2012). The May-June 2012 Ferrara Arc earthquakes (northern Italy): structural control of the spatial evolution of the seismic sequence and of the surface pattern of coseismic fractures, *Ann. Geophys.* **55**(4), 533-540.

Luzi, L., F. Pacor, G. Ameri, R. Puglia, P. Burrato, M. Massa, P. Augliera, G. Franceschina, S. Lovati, and R. Castro (2013). Overview on the strong-motion data recorded during the May–June 2012 Emilia seismic sequence, *Seism. Res. Lett.* **84**, 629-644.

Margheriti L., R. M. Azzara, M. Cocco, A. Delladio, and A. Nardi (2000). Analysis of Borehole Broadband Recordings: Test Site in the Po Basin, Northern Italy. *Bull. Seismol. Soc. Am.*, **90**, 1454–1463.

Meletti C., F. Galadini, G. Valensise, M. Stucchi, R. Basili, S. Barba, G. Vannucci, and E. Boschi (2008). A seismic source zone model for the seismic hazard assessment of the Italian territory. *Tectonophysics*, **450**, 85-108.

Norme Tecniche per le Costruzioni (2008). Decrreto 14 gennaio 208, Ministero delle Infrastrutture. Gazzetta Ufficiale n. 29 del 4-2-2008- Suppl. Ordinario n. 30.

Pacor, F., R. Paolucci, L. Luzi, F. Sabetta, A. Spinelli, A. Gorini, M. Nicoletti, S. Marcucci, L. Filippi, and M. Dolce (2011). Overview of the Italian strong motion database ITACA 1.0, *Bull. Earthq. Eng*, **9**, 1723–1739.

Perez, A., M. A. Jaimes, and M. Ordaz (2009). Spectral Attenuation Relations at Soft Sites Based on Existing Attenuation Relations for Rock Sites, *J. Earthq. Eng.* **13**, 236-251.

Pezzo G., Merryman Boncori J.P., Tolomei C., Salvi S., Atzori S., Antonioli A., Trasatti E., Novali F., Serpelloni E., Candela L., Giuliani R. (2013). Coseismic Deformation and Source Modeling of the May 2012 Emilia (Northern Italy) Earthquakes. *Seism. Res. Lett.* **84**(4), 645-655.

Rathje, E., A. Kottke, and W. Trent (2010). Influence of Input Motion and Site Property Variabilities on Seismic Site Response Analysis, *ASCE J. Geotech. Geoenviron. Eng.* **136**(4), 607–619.

Rodríguez-Marek, A., Montalva, G., Cotton, F. and Bonilla, F. (2011). Analysis of single-station standard deviation using the KiK-net data, *Bull. Seismol. Soc. Am.* **101**(3), 1242–1258.

Rodríguez-Marek, A., F. Cotton, N. A. Abrahamson, S. Akkar, L. Al Atik, B. Edwards, G. A. Montalva, and H. Dawood (2013). A model for single-station standard deviation using data from various tectonic regions, *Bull. Seismol. Soc. Am.* **103**, 3149–3163.

Rodríguez-Marek A., Rathje E. M., Bommer J. J., Scherbaum F., and Stafford P. J. (2014), Application of Single-Station Sigma and Site-Response Characterization in a Probabilistic Seismic-Hazard Analysis for a New Nuclear Site, *Bull. Seismol. Soc. Am.*, **104**(4), doi: 10.1785/0120130196.

Rovida, A., R. Camassi, P. Gasperini, M. Stucchi (eds.), 2011. CPTI11, the 2011 version of the Parametric Catalogue of Italian Earthquakes. Milano, Bologna, http://emidius.mi.ingv-it/CPTI.

Scognamiglio, L., L. Margheriti, F. M. Mele, E. Tinti, A. Bono, P. De Gori, V. Lauciani, F. P. Lucente, A. G. Mandiello, C. Marcocci, S. Mazza, S. Pintore, and M. Quintiliani (2012). The 2012 Pianura Padana Emiliana seismic sequence: Locations, moment tensors and magnitudes, *Ann. Geophys.* **55** (4), 549-559.

Seed, H. B., and I. M. Idriss (1970). Soil Moduli and Damping Factors for Dynamic Response Analysis, Technical Report UCB/EERC-70/10, Earthquake Engineering Research Center, University of California, Berkeley, 48 pp.

Smerzini C., C. Galasso, I. Iervolino, and R. Paolucci (2014). Ground motion record selection based on broadband spectral compatibility, *Earthquake Spectra*, **30**, 1427–1448 .

Zhao, J. X., J. Zhang, A. Asano, Y. Ohno, T. Oouchi, T. Takahashi, H. Ogawa, K. Irikura, H.K. Thio, P.G. Somerville, and Y. Fukushima (2006). Attenuation relations of strong ground motion in Japan using site classification based on predominant period. *Bull. Seismol. Soc. Am.*, **96**(3), 898–913.

Full mailing address for each author

Ezio Faccioli, e.faccioli@studiogeotecnico.it

Via Giuseppe Ripamonti, 89, Milano, Italy

Roberto Paolucci, roberto.paolucci@polimi.it

Piazza Leonardo da Vinci 32, 20133 Milano, Italy

Manuela Vanini, mm.vanini@gmail.com

Via G.B. Moroni 160, 24122 Bergamo, Italy

Tables

Table 1 – Classes of approaches to account for site effects in PSHA.

Hybrid probabilistic/deterministic		**Fully probabilistic**		
Generic site	*Site-specific*	*Generic site*	*Site-specific*	
HyG PSHA at rock + SAF based on seismic norms	***HyS*** PSHA at rock + SAF based on site-specific soil response analyses (typically 1D)	***FpG*** PSHA based on GMPE with site correction factors	***FpS-1*** PSHA at site with single-station sigma applied	***FpS-2*** PSHA at rock with single-station sigma convolved with SAF probability function conditioned to rock ground motion.

Table 2 – Weights assigned to the three sigma level branches of the adopted Logic Tree, shown in Figure 6.

weights	Ground type C		Ground type A
Sigma level branch	MRN/T0821	NVL	all
$\sigma_{ss,s}^{u}$	0.2	0.1	0.1
$\sigma_{ss,s}$	0.5	0.4	0.4
$\sigma_{ss,s}^{l}$	0.3	0.5	0.5

Table 3 – Accelerograms selected for propagation analyses, for 475 and 2475 yrs.

RP	id	Station name	Country	Event date and time	M_w	R_{epi} (km)	PGA (cm/s^2)	PGV (cm/s)	site	*Vs30* (m/s)
475	1	Tarcento (WE)	Italy	1976.09.15 (09:21)	5.9	10.0	100.4	4.0	A	901
	2	AKT012 (NS)	Japan	1998.09.03 (07:58)	5.9	20.5	101.5	2.5	B	384
	3	Hella (EW)	Iceland	2000.06.21 (00:51)	6.4	21.4	110.0	6.1	B	na
	4	TKY011 (EW)	Japan	2000.07.30 (00:18)	5.7	18.7	119.9	8.4	B	408
	5	NIG021 (NS)	Japan	2011.03.11 (19:32)	5.6	25.2	113.1	3.4	B	412
	6	FKS010 (EW)	Japan	2011.03.22 (22:12)	5.7	25.4	66.6	4.4	B	409
	7	FKS015 (NS)	Japan	2011.04.12 (05:07)	5.9	23.9	76.2	6.7	B	601
2475	1	Cerro Prieto (H2)	USA	1979.10.15 (23:16)	6.5	24.7	165.8	11.6	B	660
	2	Minni-Nupur (NS)	Iceland	2000.06.17 (15:40	6.5	13.2	155.9	11.3	A	na
	3	Solheimar (NS)	Iceland	2000.06.17 (15:40)	6.5	17.4	241.2	9.7	B	na
	4	Hella (NS)	Iceland	2000.06.21 (00:51)	6.4	21.4	165.1	9.8	B	na
	5	TKY011 (NS)	Japan	2000.07.30 (12:25)	6.4	21.6	196.4	9.9	B	408
	6	Selfoss-Hospital (NS)	Iceland	2008.05.29 (15:45)	6.3	8.0	210.3	17.4	A	na
	7	NIG021 (EW)	Japan	2011.03.11 (18:59)	6.2	20.7	246.5	11.1	B	412

Table 4 – Soil profile for parametric analyses on the effect of the non-linear soil modelling. Ish93 (Ishibashi and Zhang, 1993); S&I70 (Seed and Idriss, 1970); Dar01 (Darendeli, 2001).

Thickness [m]	**Soil material**	**γ[kN/m^3]**	**Vs [m/s]**	**Non-linear curves for G/G_{max} and ξ**			
12.0	Clay	18.0	180	Ish93	S&I70	San Carlo (clay)	Dar01
18.0	Sand	18.0	270	Ish93	S&I70	Fioravante (sand)	Dar01
10.0	Sand	18.0	475	Ish93	S&I70	Fioravante (sand)	Dar01
25.0	Sand	18.0	288	Ish93	S&I70	Fioravante (sand)	Dar01
35.0	Sand	18.0	400	Ish93	S&I70	Fioravante (sand)	Dar01
	rock	20.0	800				

Table 5 – Synthesis of results presented in this paper to quantify the epistemic uncertainty related to 1D soil modelling, with representative values of σ_{log10} as a function of the period range. The first column reports results for RP= 475 yrs and the second for RP = 2475 yrs. In the last row, the corresponding values obtained from the analysis of SAFs at 21 deep soil sites in the Kik-net are also shown as a reference.

APPROACH		Short periods (< 0.5 s)		Intermediate periods (0.5 - 2 s)		Long periods (> 2s)	
		RP 475	RP 2475	RP 475	RP 2475	RP 475	RP 2475
	$\sigma_{Kik\text{-}net}$	0.10		0.08		0.08	
	σ_{PSHA_rock} (***)	0.12	0.08	0.08	0.05	0.03	0.06
	σ_{input_1D}	Minor contribution to σ, provided that input motions are matched to the rock PSHA spectrum at the selected return period.					
LIN	$\sigma_{Vs} \equiv \sigma_{epistemic\_1D}$ (all profiles and all input THs = 49 analyses)	0.05	0.07	0.05	0.06	0.03	0.02
	$(\sigma^2_{epistemic\_1D} + \sigma^2_{PSHA\_rock})^{0.5}$	0.13	0.11	0.09	0.07	0.05	0.07
	$\sigma_{TOT\ LIN}$	0.13	0.11	0.09	0.08	0.08	0.08
EQL	σ_{Vs} (all profiles, 7x7 analyses)	0.05	0.06	0.05	0.07	0.04	0.04
	σ_{Soil_Model} (1 profile, 7x4 analyses)	0.07	0.11	0.06	0.09	0.04	0.04
	$\sigma_{epistemic\_1D} = (\sigma^2_{Vs} + \sigma^2_{SM})^{0.5}$	0.09	0.12	0.08	0.11	0.05	0.05
	$(\sigma^2_{epistemic\_1D} + \sigma^2_{PSHA\_rock})^{0.5}$	0.15	0.15	0.11	0.12	0.06	0.08
	$\sigma_{TOT\ EQL}$	0.15	0.15	0.11	0.12	0.08	0.08
NL	σ_{Vs} (all profiles, 7x7 analyses)	0.06	0.05	0.08	0.06	0.04	0.04
	σ_{Soil_Model} (1 profile, 7x4 analyses)	0.08	0.13	0.07	0.10	0.04	0.04
	$\sigma_{epistemic\_1D} = (\sigma^2_{Vs} + \sigma^2_{SM})^{0.5}$	0.10	0.14	0.10	0.11	0.05	0.06
	$(\sigma^2_{epistemic\_1D} + \sigma^2_{PSHA\_rock})^{0.5}$	0.16	0.17	0.13	0.12	0.06	0.09
	$\sigma_{TOT\ NL}$	0.16	0.17	0.13	0.12	0.08	0.09

(***) computed as: $(\log_{10}(UHS_{84\text{-}perc})-\log_{10}(UHS_{16\text{-}perc}))/2$

List of Figure Captions

Figure 1 – Map of Northern Italy (in background), where Po Plain extends roughly between Torino and Venezia, with earthquake epicenters (*Mw*≥ 4.0) from working catalogue (1005-2013) discussed in Faccioli (2013). Triangles show the accelerometer sites considered in this study. Polygons with continuous lines are the surface projections of the Area Sources (ASs) taken from the ZS9 model of Meletti et al. (2008), with corresponding number, while polygons with dashed lines show changes introduced in Faccioli (cit.). SPP = Southern Po Plain AS, grouping together the ZS9 912, 913, and 914 ASs. Polygon labelled "slab" is the surface projection of an inclined "slab zone", to which the deep events have been associated in Faccioli (cit.). Stars denote the most recent regional events with M_w>4.

Figure 2 – (a) DEM of Po Plain portion with accelerometer and other sites of interest, showing also depth contours of the base of early Pliocene (M-P_1 in (b)), from Bigi et al., 1992. Rupture area projections of the Reggio Emilia 1996 and the two Emilia 2012 mainshocks are also shown as black rectangles. Selected sites used in subsequent analyses are marked with a white circle. (b) Geological profile interpreted from seismic reflection data, adapted after Boccaletti et al. (2010) corresponding to trace B-B' in (a) (black line). Ca: Meso-Cenozoic (carbonatic succession); M: Miocene; M-P_1: Late Messinian (Early Pliocene); Qm: Early Pleistocene; a: Middle Pleistocene-Holocene; b: Middle Pleistocene; P_2: Middle-Late Pliocene.

Figure 3 – Representative types of *Vs* profiles in Po Plain: (left) with strong impedance contrast at 80-to-120 m depth, (right) without strong contrast in the upper 200 m or so. NVL and MDN profiles are from ITACA 2.0; T0821 and MRN profiles are from Progetto S2 (2012); the other profiles are from Albarello et al. (2011). Shaded areas show mean +/- 1 Stdev bands of corresponding groups of profiles. (See Data and Resources section for cited references).

Figure 4 – (*left*) Event and site corrected single-station sigma, $\phi_{ss,s}$, and (*right*) site factor $\delta S2S$ for the set of 12 representative accelerometer sites on deep soil deposits listed in the legend, shown also in Figure 3. The inter-event component (τ_{log10} ITA13) of the standard deviation of ITA13 GMPE is also shown on the graph at left.

Figure 5 – (*left*) Site terms δS2S for the three study sites with ± 1 $\sigma_{S2S\ epistemic}$ bands estimated through (4). (*right*) Total single-site sigma, $\sigma_{ss,s}$, for the same sites (solid lines), with upper and lower variability limits (dashed lines) estimated from (5); the ITA13 GMPE standard deviation (σ_{log10} ITA13) is also shown in this plot. The variability estimates are in both cases associated to the 12-site Po Plain subset.

Figure 6 – Logic Tree used for SH computations. "Modified ITA13" refers to (3), with no variability associated to $\delta S2S$, as explained in text. $\phi_{ss,s}$ values in all branches are the site specific ones, while the stdev $\phi_{ss,s}$ are computed over the Po Plain subset. The weights assigned to the sigma level branches are listed in Table 2, the weights of the earthquake source model branches are shown in the figure, for the two adopted return periods (RP): note the change in weights when RP increases to 2475 years.

Figure 7 – Uniform Hazard, 5% damped acceleration response spectra obtained for the NVL (*left*) and MRN (*right*) study sites from the six branches of the Logic Tree of Figure 6. Dash-dot lines are spectra from actual records, while smooth solid curves are current code spectra (NTC2008) for Eurocode 8 class C subsoil category.

Figure 8 – Percentile UHS, and mean spectra calculated for the three study sites using the Logic Tree of Figure 6, with the return periods shown. Note low spectral ordinates at T0821 with respect to MRN and NVL. This is related to the corresponding low δS2S value (see Figure 5).

Figure 9 – (*Left*) Accelerometer stations on ground type A within about 75 and 120 km from the study area (May 2012 events); white stars denote the main events of the Emilia 2012 sequence. (*Right*) Site terms for the 21 stations with at least 5 records within the light gray circle in the left map, with mean $\pm 1\sigma$ band (shaded) .

Figure 10 – (*Left*) Regional ϕ_{ss} value for rock sites, mean +- 1stdrd.dev. and median, based on the 120 km dataset restricted to sites with a minimum of 5 records. (*Right*) Regional single-station sigma range for rock sites compared with the standard deviation of ITA13.

Figure 11 - Percentile UHS, and mean spectra spectra calculated for the three study sites for exposed bedrock (ground type A) using the Logic Tree of Figure 6, with the return periods shown. Thin gray lines are current code (NTC2008) spectra for Eurocode 8 (CEN, 2003) class A subsoil category.

Figure 12 - Results of spectral matching for representative selected records RP = 475 yrs (left) and RP = 2475 yrs (right). Top: Comparison in terms of acceleration response spectra (thin black: RS of the original record; dashed grey: target spectrum; thick black: RS of the spectrally matched record; 15 iterations have been performed). Bottom: time-histories of acceleration, velocity and displacement (thick grey: original record; thin black: corrected record). It is noted that broadband compatibility implies a modest adjustment at long periods, thus preserving the physical nature of the original record.

Figure 13 - *Vs* profiles at several sites in the Mirandola urban area. Data from Project S2 (2000). Range of variability from a set of surface-waves inversion based *Vs* profiles at MRN accelerometric station site (S. Foti, personal communication) is also shown shaded in light grey (right). The 'Martelli' profile, from Project S2 (2000), is a consensus profile for the Southern part of Mirandola urban area. (See Data and Resources for cited references).

Figure 14 - Left: average acceleration response spectra resulting from different Vs profiles and different sets of input motions, either unscaled or scaled in the 0-1 s or 0-5 s period ranges. Right: corresponding sigma in log10 scale. RP=475 yrs, equivalent-linear analyses.

Figure 15 - G/G_{max} -γ and ξ–γ curves for clay soil at 6 m depth (left) and sandy soil at 52.5 m depth (right).

Figure 16 - Acceleration response spectra at Mirandola obtained using the soil profile of Table 4 and the input accelerograms for RP = 475 yrs (scaled with spectral matching up to 5 s). On the left, results based on the linear equivalent approach; on the right, results based on a fully non-linear approach.

Figure 17 - Comparison of average response spectra computed for MRN site with the Vs profile of Table 4, in the linear visco-elastic case (quality factor $Q=Vs/10$) and in the non-linear case by the "Fioravante model", considering both linear-equivalent and non-linear approach. RP = 475 yrs is considered on the left and RP = 2475 yrs on the right plots. The black thick line depicts the UHS spectrum at Mirandola for class C soil obtained through the one-step fully probabilistic approach illustrated in this paper (see Figure 8). Spectra from MRN records are also shown.

Figure 18 - Spectral amplification functions computed at NIGH11 (top) and IWTH20 (bottom) Kik-net stations, as the ratio of response spectral amplitude at ground surface with respect to the corresponding amplitude at the borehole station about 200 m depth. Data are disaggregated according to the amplitude of motion at the borehole station, measured by the pseudo-velocity PSV at the corresponding period. Data are grouped by Magnitude. White dots: $M<4$, light grey: $4<M<5$; dark grey: $5<M<6$; black: $M>6$.

Figure 19 Comparison of response spectra from linear (dark grey) and fully non-linear (light grey) analyses and UHS from soil category C analyses (thick dashed black lines), for the MRN site. Mean plus and minus one standard deviation bands are shaded. Stdrd. dev. values are the σ_{TOT} of Table 5.

Figures

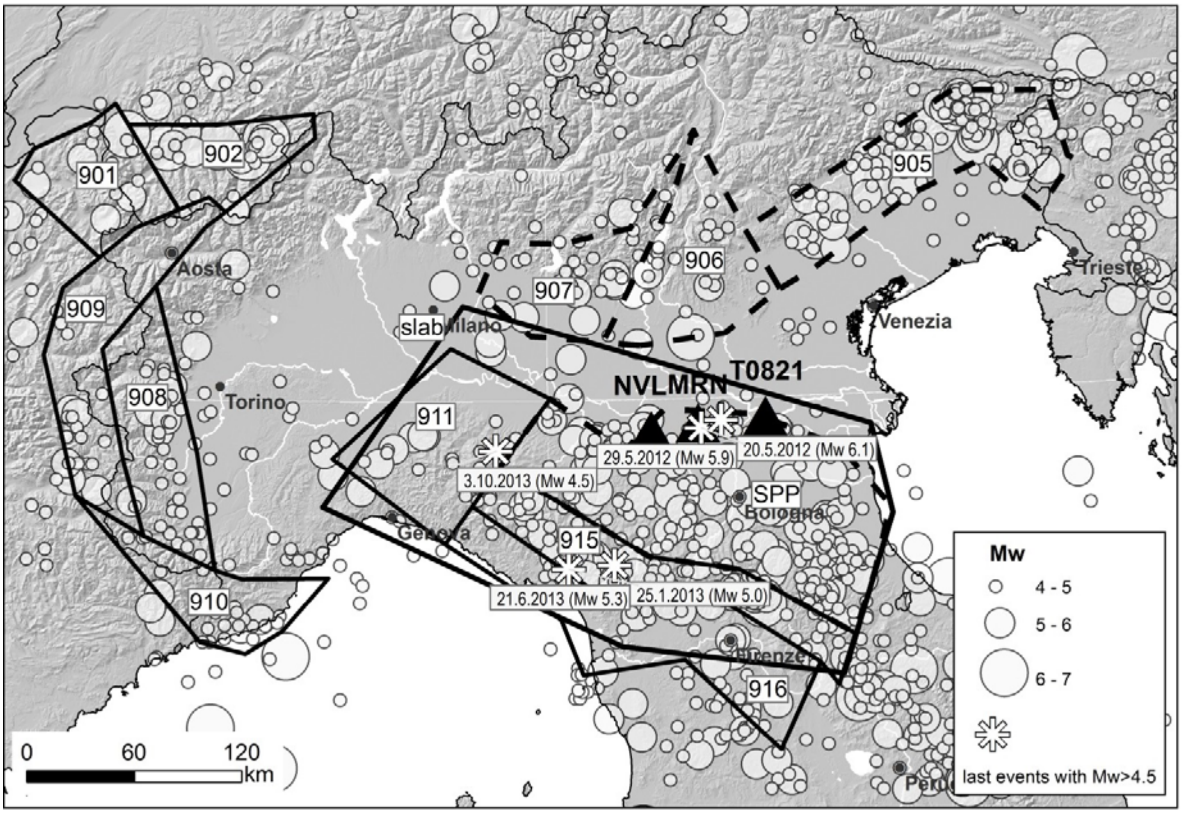

Figure 1 – Map of Northern Italy (in background), where Po Plain extends roughly between Torino and Venezia, with earthquake epicenters (Mw≥ 4.0) from working catalogue (1005-2013) discussed in Faccioli (2013). Triangles show the accelerometer sites considered in this study. Polygons with continuous lines are the surface projections of the Area Sources (ASs) taken from the ZS9 model of Meletti et al. (2008), with corresponding number, while polygons with dashed lines show changes introduced in Faccioli (cit.). SPP = Southern Po Plain AS, grouping together the ZS9 912, 913, and 914 ASs. Polygon labelled “slab” is the surface projection of an inclined “slab zone”, to which the deep events have been associated in Faccioli (cit.). Stars denote the most recent regional events with M_w>4.

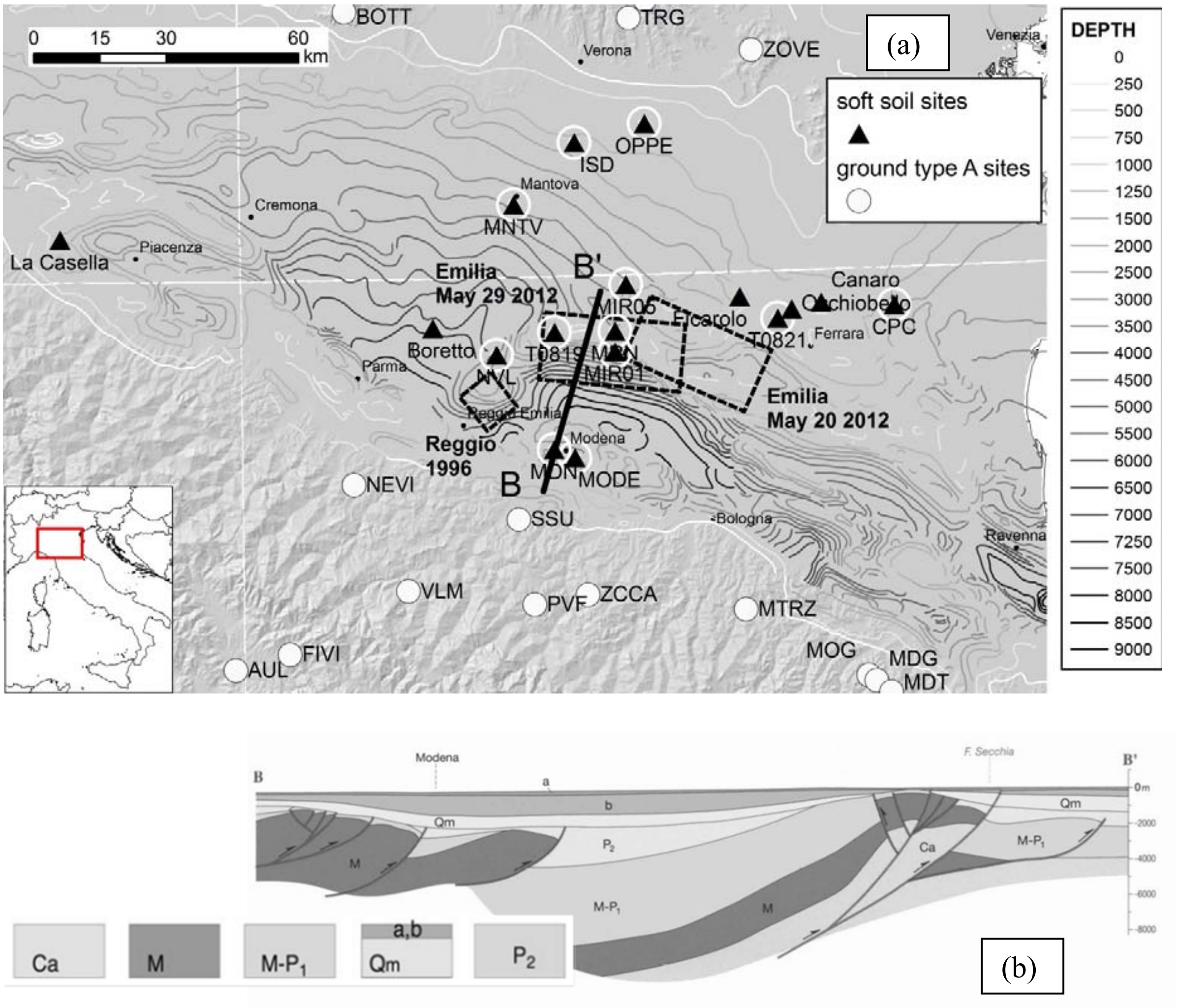

Figure 2 – (a) DEM of Po Plain portion with accelerometer and other sites of interest, showing also depth contours of the base of early Pliocene (M-P_1 in (b)), from Bigi et al., 1992. Rupture area projections of the Reggio Emilia 1996 and the two Emilia 2012 mainshocks are also shown as black rectangles. Selected sites used in subsequent analyses are marked with a white circle. (b) Geological profile interpreted from seismic reflection data, adapted after Boccaletti et al. (2010) corresponding to trace B-B’ in (a) (black line). Ca: Meso-Cenozoic (carbonatic succession); M: Miocene; M-P_1: Late Messinian (Early Pliocene); Qm: Early Pleistocene; a: Middle Pleistocene-Holocene; b: Middle Pleistocene; P_2: Middle-Late Pliocene.

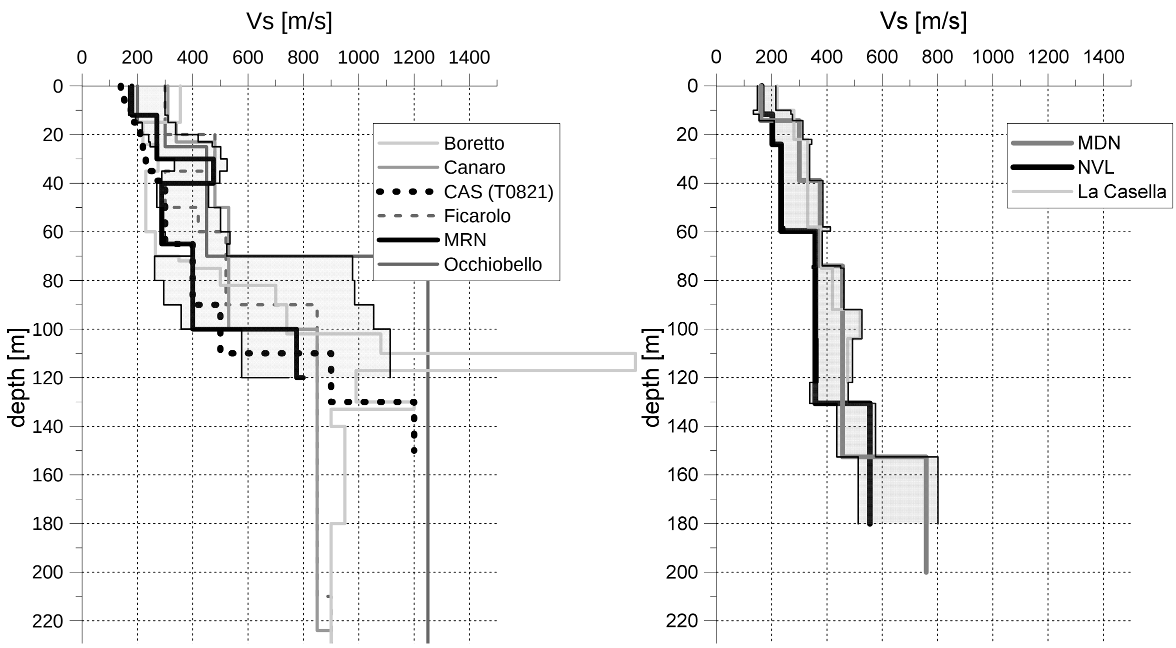

Figure 3 – Representative types of Vs profiles in Po Plain: (left) with strong impedance contrast at 80-to-120 m depth, (right) without strong contrast in the upper 200 m or so. NVL and MDN profiles are from ITACA 2.0; T0821 and MRN profiles are from Progetto S2 (2012); the other profiles are from Albarello et al. (2011). Shaded areas show mean +/- 1 Stdev bands of corresponding groups of profiles. (see Data and Resources section for cited references).

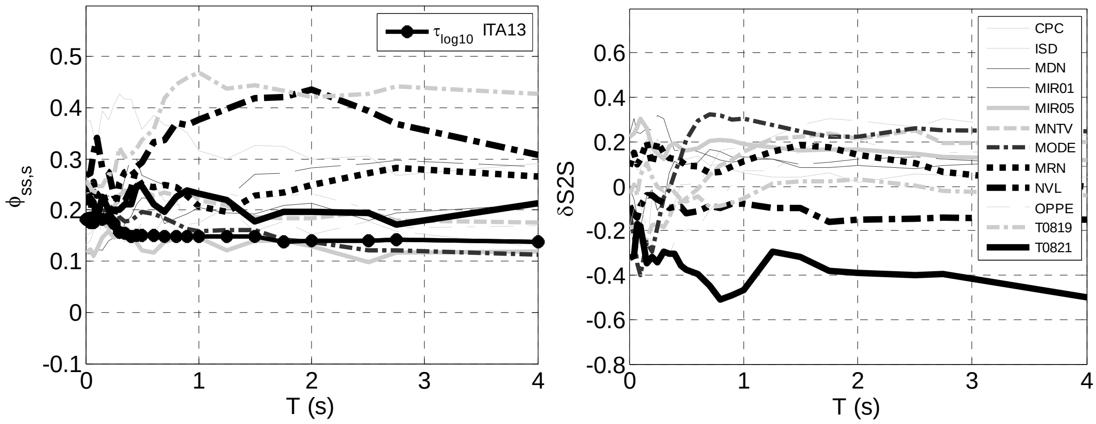

Figure 4 – (*left*) Event and site corrected single-station sigma, $\phi_{ss,s}$, and (*right*) site factor $\delta S2S$ for the set of 12 representative accelerometer sites on deep soil deposits listed in the legend, shown also in Figure 3. The inter-event component (τ_{log10} ITA13) of the standard deviation of ITA13 GMPE is also shown on the graph at left.

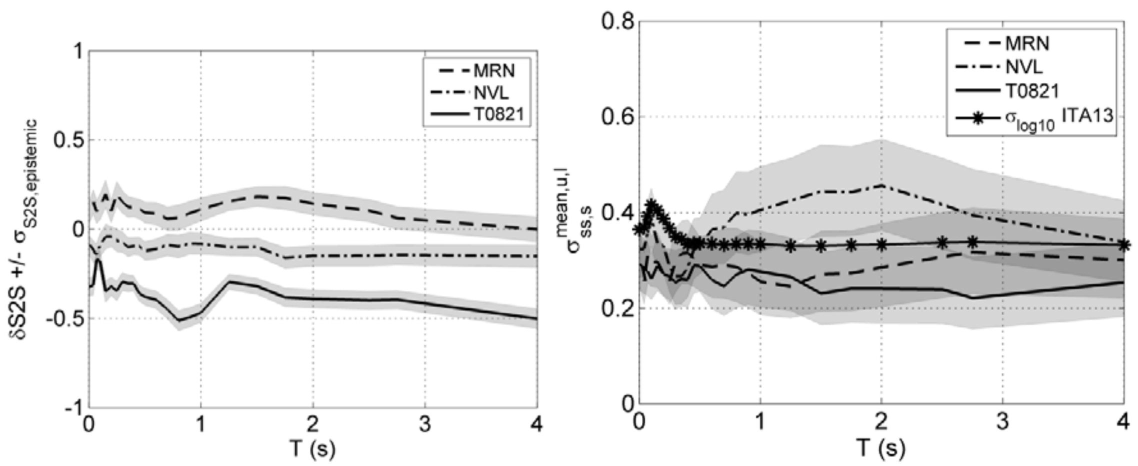

Figure 5 – (*left*) Site terms δS2S for the three study sites with ± 1 $\sigma_{S2S\ epistemic}$ bands estimated through (4). (*right*) Total single-site sigma, $\sigma_{ss,s}$, for the same sites (solid lines), with upper and lower variability limits (dashed lines) estimated from (5); the ITA13 GMPE standard deviation (σ_{log10} ITA13) is also shown in this plot. The variability estimates are in both cases associated to the 12-site Po Plain subset.

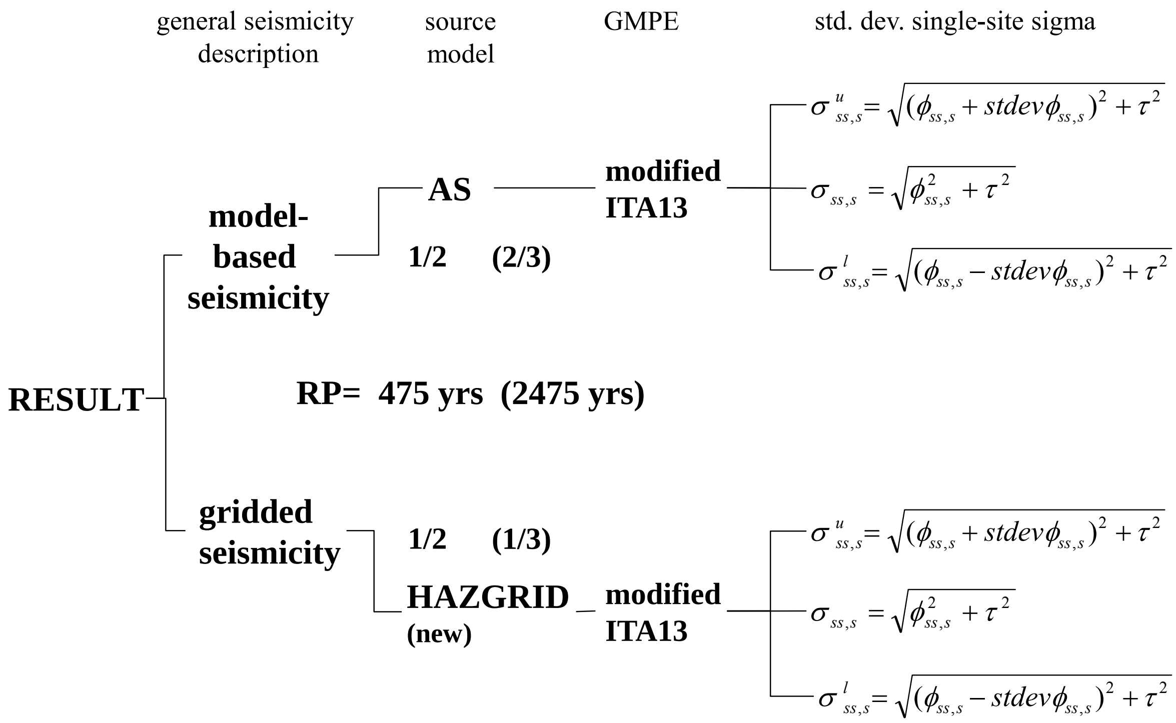

Figure 6 – Logic Tree used for SH computations. "Modified ITA13" refers to (3), with no variability associated to $\delta S2S$, as explained in text. $\phi_{ss,s}$ values in all branches are the site specific ones, while the stdev $\phi_{ss,s}$ are computed over the Po Plain subset. The weights assigned to the sigma level branches are listed in Table 2, the weights of the earthquake source model branches are shown in the figure, for the two adopted return periods (RP): note the change in weights when RP increases to 2475 years.

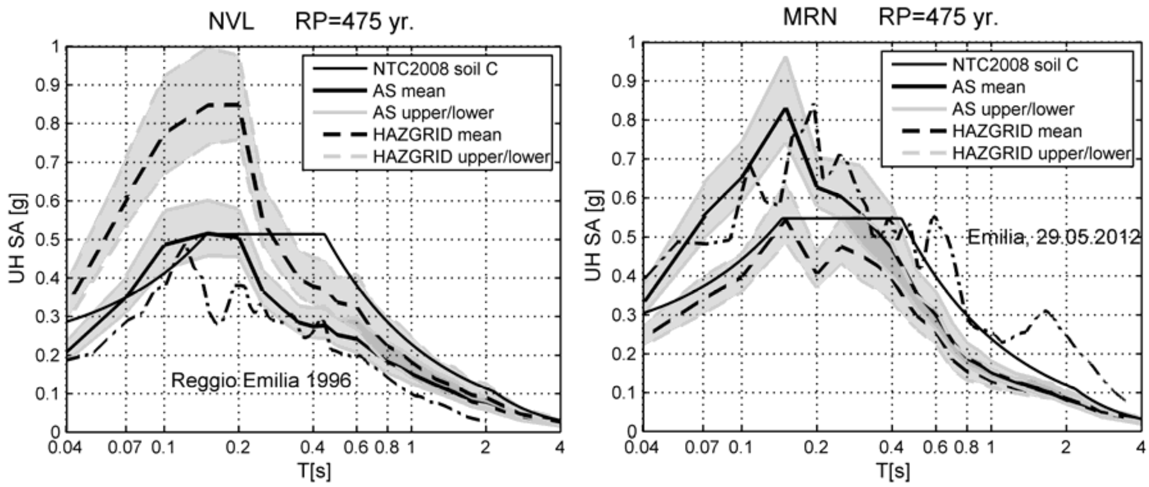

Figure 7 – Uniform Hazard, 5% damped acceleration response spectra obtained for the NVL (*left*) and MRN (*right*) study sites from the six branches of the Logic Tree of Figure 6. Dash-dot lines are spectra from actual records, while smooth solid curves are current code spectra (NTC2008) for Eurocode 8 class C subsoil category.

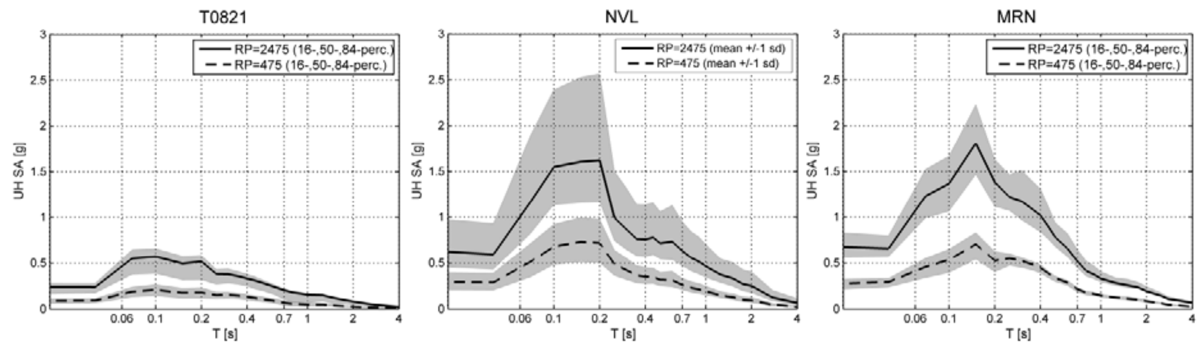

Figure 8 – Percentile UHS, and mean spectra calculated for the three study sites using the Logic Tree of Figure 6, with the return periods shown. Note low spectral ordinates at T0821 with respect to MRN and NVL. This is related to the corresponding low δS2S value (see Figure 5) .

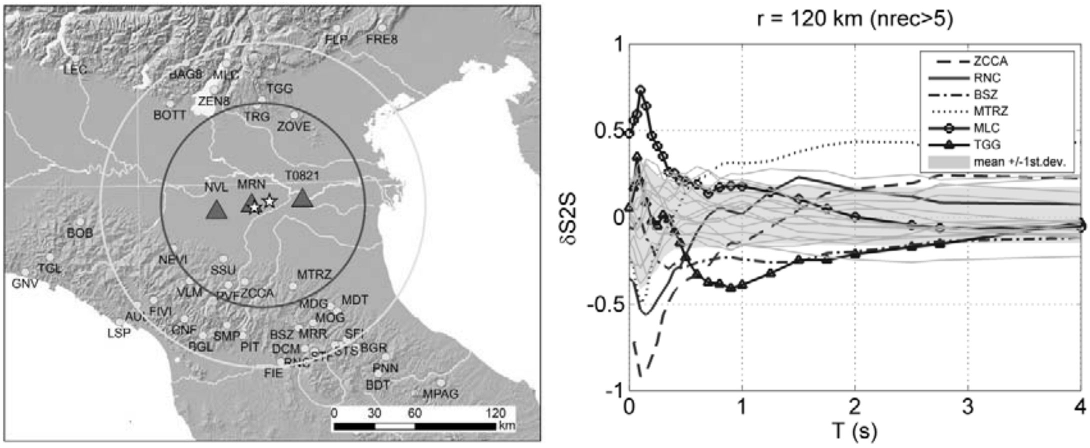

Figure 9 – (*Left*) Accelerometer stations on ground type A within about 75 and 120 km from the study area (May 2012 events); white stars denote the main events of the Emilia 2012 sequence. (*Right*) Site terms for the 21 stations with at least 5 records within the light gray circle in the left map, with mean $\pm 1\sigma$ band (shaded).

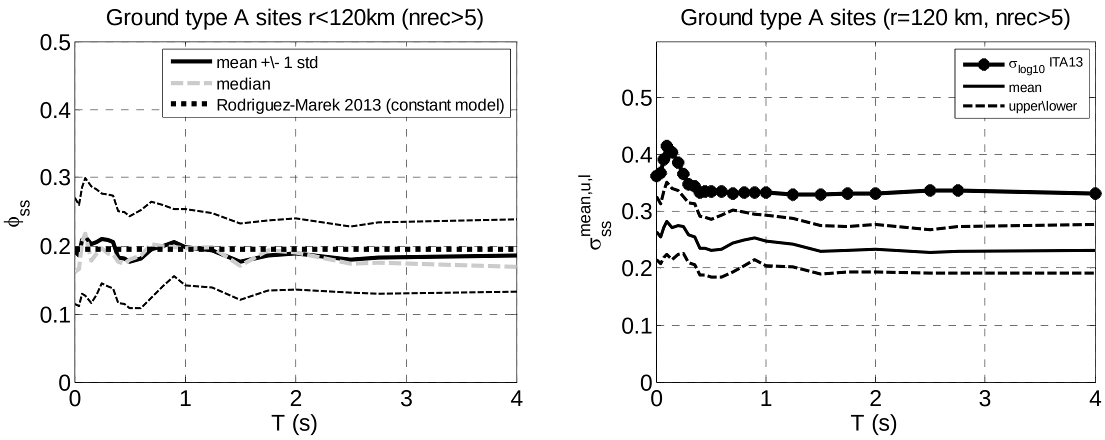

Figure 10 – (*Left*) Regional ϕ_{ss} value for rock sites, mean +- 1stdrd.dev. and median, based on the 120 km dataset restricted to sites with a minimum of 5 records. (*Right*) Regional single-station sigma range for rock sites compared with the standard deviation of ITA13.

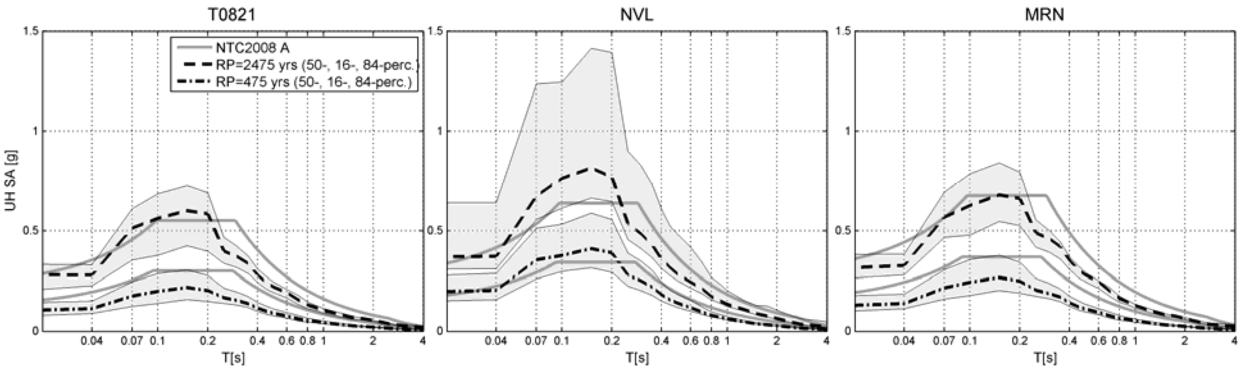

Figure 11 - Percentile UHS spectra calculated for the three study sites for exposed bedrock (ground type A) using the Logic Tree of Figure 6, with the return periods shown. Thick gray lines are current code (NTC2008) spectra for Eurocode 8 (CEN, 2003) class A subsoil category.

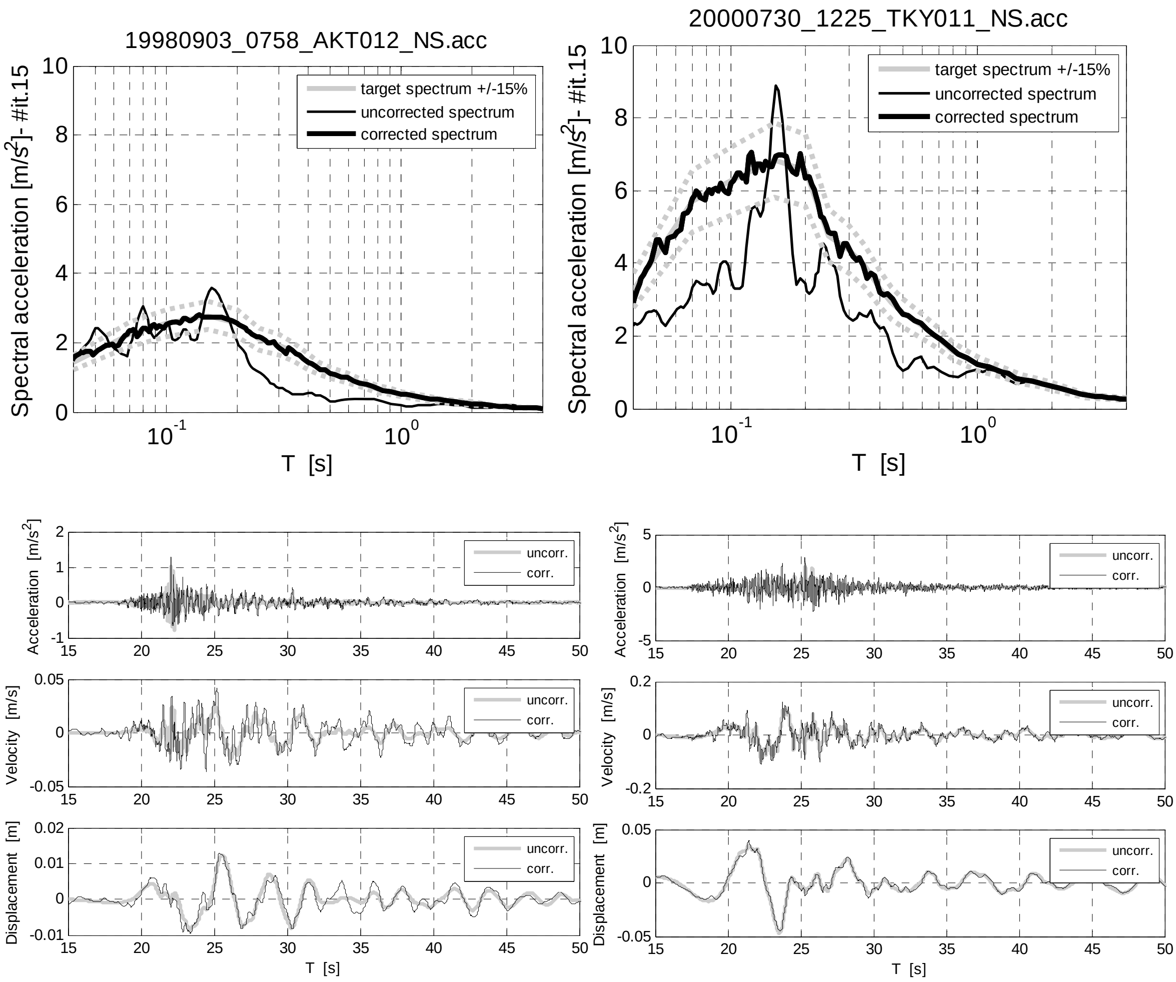

Figure 12 - Results of spectral matching for representative selected records RP = 475 yrs (left) and RP = 2475 yrs (right). Top: Comparison in terms of acceleration response spectra (thin black: RS of the original record; dashed grey: target spectrum; thick black: RS of the spectrally matched record; 10 iterations have been performed). Bottom: time-histories of acceleration, velocity and displacement (thick grey: original record; thin black: corrected record). It is noted that broadband compatibility implies a modest adjustment at long periods, thus preserving the physical nature of the original record.

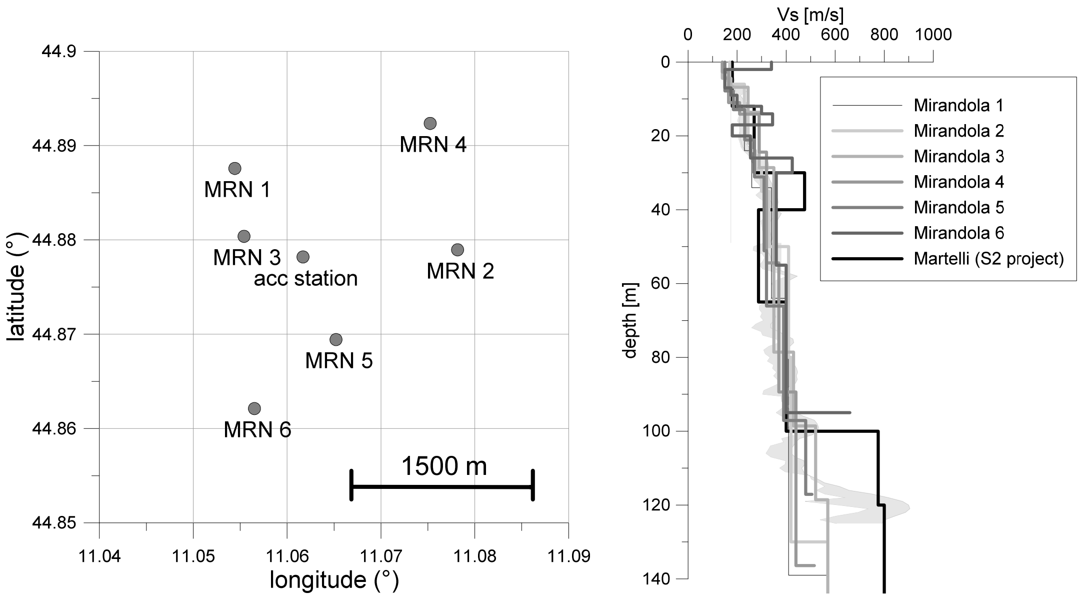

Figure 13 - Vs profiles at several sites in the Mirandola urban area. Data from Project S2 (2000). Range of variability from a set of surface-waves inversion based Vs profiles at MRN accelerometric station site (S. Foti, personal communication) is also shown shaded in light grey (right). The 'Martelli' profile, from Project S2 (2000), is a consensus profile for the Southern part of Mirandola urban area. (see Data and Resources section for cited references).

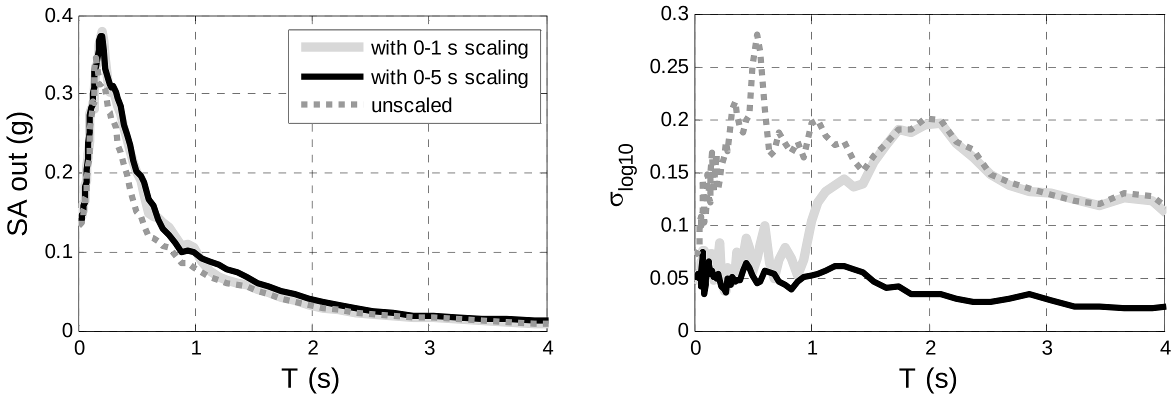

Figure 14 - Left: average acceleration response spectra resulting from different Vs profiles and different sets of input motions, either unscaled or scaled in the 0-1 s or 0-5 s period ranges. Right: corresponding sigma in log10 scale. RP=475 yrs, equivalent-linear analyses.

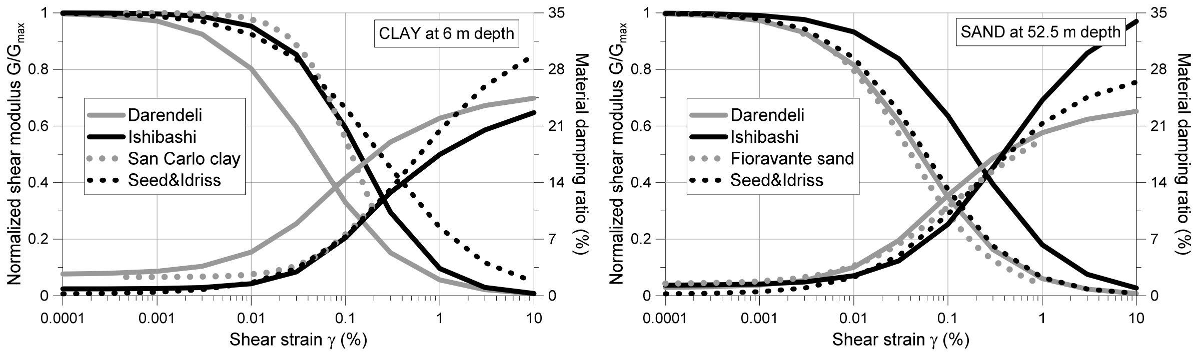

Figure 15 - G/G_{max} -γ and ξ–γ curves for clay soil at 6 m depth (left) and sandy soil at 52.5 m depth (right).

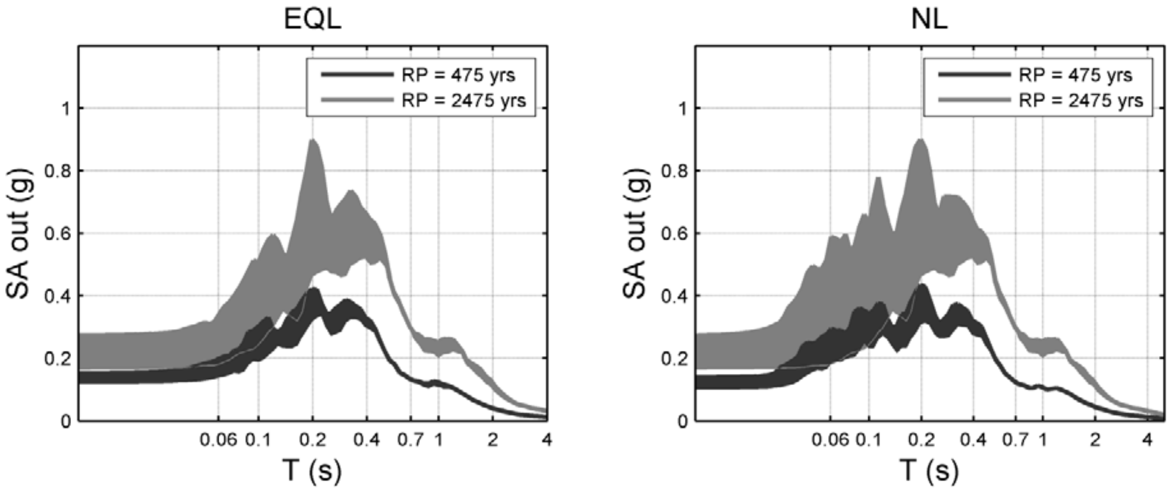

Figure 16 - Acceleration response spectra at Mirandola obtained using the soil profile of Table 4 and the input accelerograms for RP = 475 yrs (scaled with spectral matching up to 5 s). On the left, results based on the linear equivalent approach; on the right, results based on a fully non-linear approach.

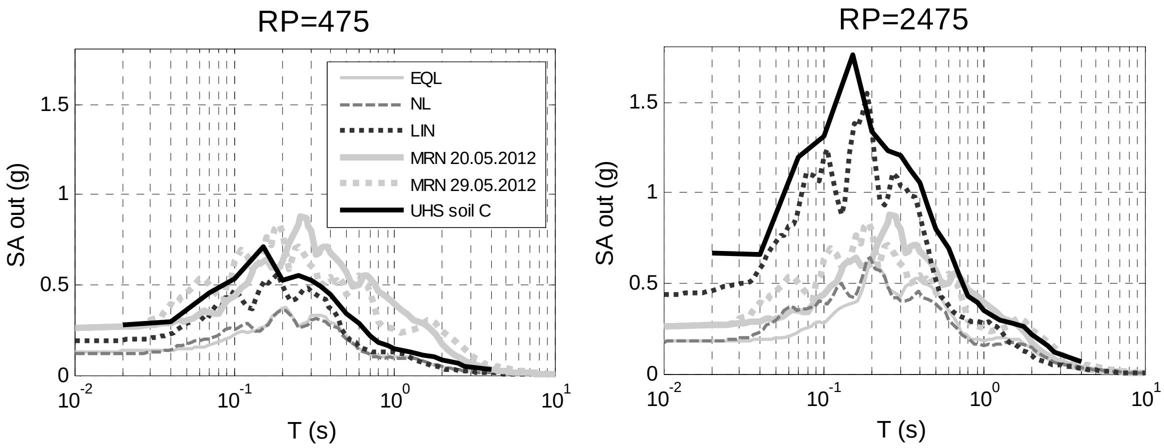

Figure 17 - Comparison of average response spectra computed for MRN site with the *Vs* profile of Table 4, in the linear visco-elastic case (quality factor *Q=Vs/10*) and in the non-linear case by the "Fioravante model", considering both linear-equivalent and non-linear approach. RP = 475 yrs is considered on the left and RP = 2475 yrs on the right plots. The black thick line depicts the UHS spectrum at Mirandola for class C soil obtained through the one-step fully probabilistic approach illustrated in this paper (see Figure 8). Spectra from MRN records are also shown.

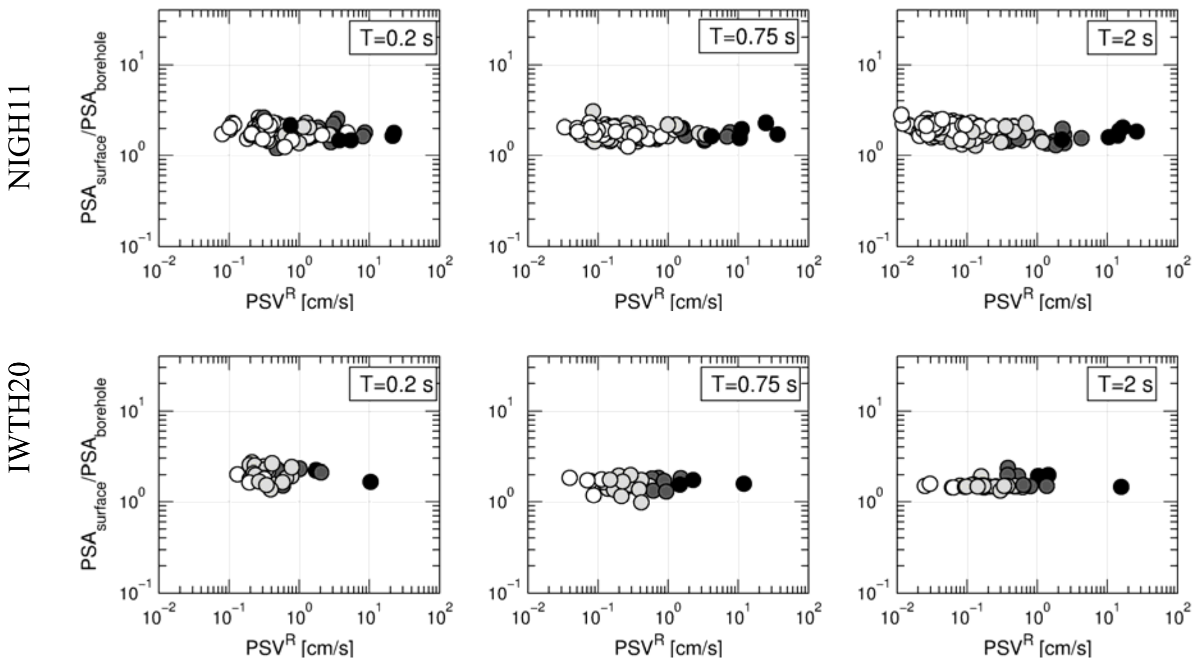

Figure 18 - Spectral amplification functions computed at NIGH11 (top) and IWTH20 (bottom) Kik-net stations, as the ratio of response spectral amplitude at ground surface with respect to the corresponding amplitude at the borehole station about 200 m depth. Data are disaggregated according to the amplitude of motion at the borehole station, measured by the pseudo-velocity PSV at the corresponding period. Data are grouped by Magnitude. White dots: $M<4$, light grey: $4<M<5$; dark grey: $5<M<6$; black: $M>6$.

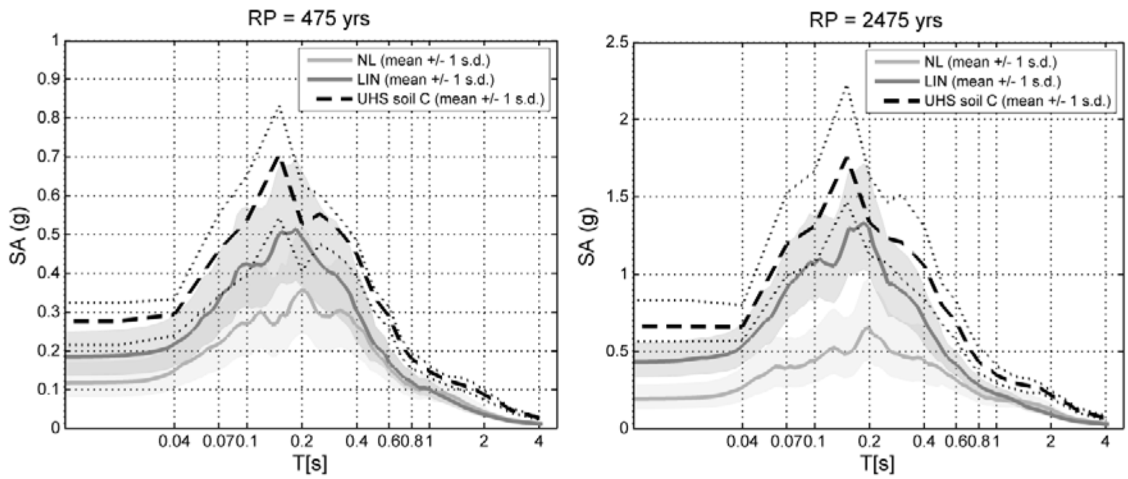

Figure 19 – Comparison of response spectra from linear (dark grey) and fully non-linear (light grey) analyses and UHS from soil category C analyses (thick dashed black lines), for the MRN site. Mean plus and minus one standard deviation bands are shaded. Stdrd. dev. values are the σ_{TOT} of Table 5

Appendix 1

Table A1 - Gutenberg-Richter *b*-values (with standard error $\sigma(b)$) used in PSHA analyses, maximum magnitude M_{max} and total occurrence rates λ associated to ASs of modified ZS9 model in Figure 1, from Faccioli (2013) with slight modifications. Last column gives percentage of total rate assigned to SSZs at different depths

AS	b	$\sigma(b)$	M_{max}	M_{max} uncertainty	Total annual rate, evts /yr $\lambda(M \geq 4.5)$	AS Depth (km)	%
901	0.84910	0.26670	6.5	0.4	0.0434	10	100
902	0.65230	0.16230	6.5	0.4	0.0916	10	100
905	1.03150	0.08620	-	-	0.4197 (total)	-	-
			5.0	0.3	0.08394	4	20
			5.8	0.3	0.25183	6	60
			6.7	0.3	0.08394	10	20
906	1.28550	0.24650	-	-	0.0904 (total)	-	-
			5.8	0.3	0.02711	6	30
			6.7	0.3	0.04519	9	50
			6.7	0.3	0.01808	15	20
907	1.16270	0.19810	-	-	0.1254 (total)	-	-
			5.0	0.3	0.02509	4	20
			5.8	0.3	0.02509	6	20
			6.7	0.3	0.03763	9	30
			6.7	0.3	0.01254	13	10
			6.7	0.3	0.01254	17	10
			6.7	0.3	0.01254	20	10
908	1.34290	0.26780	6.5	0.4	0.09069	10	100
909	1.32020	0.24970	6.5	0.4	0.10074	10	100
910	1.35830	0.23040	6.6	0.3	0.11042	10	100
911	1.26420	0.28620	-	-	0.0701 (total)	-	-
			5.8	0.5	0.02103	6	30
			6.5	0.5	0.02805	9	40
			6.5	0.5	0.02103	25	30
SPP = 912+913+914	1.17580	0.09420	-	-	0.5642 (total)	-	-
			5.8	0.5	0.11283	6	20
			6.5	0.5	0.22566	9	40

			6.5	0.5	0.22566	25	40
915	1.22480	0.14410	-	-	0.2601 (total)	-	-
			5.8	0.3	0.07804	6	30
			7.4	0.3	0.13007	9	50
			7.4	0.3	0.02601	16	10
			7.4	0.3	0.02601	21	10
916	1.65730	0.24710	-	-	0.1694 (total)	-	-
			5.8	0.3	0.05084	6	30
			7.4	0.3	0.10167	9	60
			7.4	0.3	0.01695	18	10
slab	0.67060	0.29850	6.5	0.5	0.02766	-	-